

Geochronologic and geochemical data from northern Hogem batholith and its surroundings, north-central British Columbia

L. Ootes, G. Jones, P. Schiarizza,
D. Milidragovic, R. Friedman, A. Camacho,
Y. Luo, A. Vezinet, D.G. Pearson, and S. Zhang



Ministry of
Energy, Mines and
Low Carbon Innovation

GeoFile 2020-01

**Ministry of Energy, Mines and Low Carbon Innovation
Mines, Competitiveness, and Authorizations Division
British Columbia Geological Survey**

Recommendation citation: Ootes, L., Jones, G., Schiarizza, P., Milidragovic, D., Friedman, R., Camacho, A., Luo, Y., Vezinet, A., Pearson, D.G., and Zhang, S., 2020. Geochronologic and geochemical data from northern Hogem batholith and its surroundings, north-central British Columbia. British Columbia Ministry of Energy, Mines and Low Carbon Innovation, British Columbia Geological Survey GeoFile 2020-01, 21p.

Front cover: Typical bedrock exposure in the Hogem batholith, Ominica Mountains. In the foreground are granitic rocks of the Mesilinka suite (Cretaceous); the more distant mountains (upper left) are dioritic rocks of the Thane Creek suite (Jurassic).

Back cover: Cathodoluminescent images of zircons from the Mesilinka suite. All show typical prismatic igneous zircon morphology, but some show cores with rim overgrowths. The zircon at the bottom right has a relatively higher U content (white) than its thin rim and the other zircons.



Ministry of
Energy, Mines and
Low Carbon Innovation



Geochronologic and geochemical data from northern Hogen batholith and its surroundings, north-central British Columbia

L. Ootes, G. Jones, P. Schiarizza,
D. Milidragovic, R. Friedman, A. Camacho,
Y. Luo, A. Vezinet, D.G. Pearson, and S. Zhang

Ministry of Energy, Mines and Low Carbon Innovation
British Columbia Geological Survey
GeoFile 2020-01



Geochronologic and geochemical data from northern Hogem batholith and its surroundings, north-central British Columbia

L. Ootes^{1a}, G. Jones^{1,2}, P. Schiarizza¹, D. Milidragovic^{1,3}, R. Friedman⁴, A. Camacho⁵, Y. Luo², A. Vezinet², D.G. Pearson², and S. Zhang⁶

¹ British Columbia Geological Survey, Ministry of Energy, Mines and Low Carbon Innovation, Victoria, BC, V8W 9N3

² Department of Earth & Atmospheric Sciences, University of Alberta, Edmonton, AB, T6G 2E3

³ Geological Survey of Canada, Vancouver, BC, V6B 5J3

⁴ Department of Geological Sciences, University of Manitoba, Winnipeg, MB R3T 2N2

⁵ Pacific Centre for Geochemical and Isotopic Research, University of British Columbia, Vancouver, BC, V6T 1Z4

⁶ Department of Earth Sciences, Carleton University, 1125 Colonel By Drive, Ottawa, ON Canada K1S 5B6

*corresponding author: Luke.Ootes@gov.bc.ca

Recommended citation: Ootes, L., Jones, G., Schiarizza, P., Milidragovic, D., Friedman, R., Camacho, A., Luo, Y., Vezinet, A., Pearson, D.G., and Zhang, S., 2020. Geochronologic and geochemical data from northern Hogem batholith and its surroundings, north-central British Columbia. British Columbia Ministry of Energy, Mines and Low Carbon Innovation British Columbia Geological Survey GeoFile 2020-01, 21p.

Abstract

Bedrock mapping in the Omineca Mountains of north-central British Columbia is supported by new geochemistry and geochronology. The data reported here are for rocks that are part of the Quesnel and Stikine terranes and, to a lesser extent, the Cache Creek terrane. Data and interpretations include assays, whole rock geochemistry that includes selected radiogenic Rb-Sr and Sm-Nd results, and 25 new U-Pb zircon crystallization ages, determined by CA-TIMS, LA-ICP-MS, and ID-TIMS (mechanical abrasion, multi-grain). These are complemented by 12 new ⁴⁰Ar/³⁹Ar (hornblende, muscovite, and biotite) laser step-heating results from eight samples. Three new detrital zircon U-Pb, TE, and Lu-Hf results are included for sedimentary rocks in the Stikine terrane. This GeoFile serves as a data repository for summaries and interpretations presented by Ootes et al. (2020a,b), Jones et al. (2021), and forthcoming studies.

Keywords: Hogem batholith; Quesnel terrane; Stikine terrane; geochemistry; U-Pb zircon crystallization ages; detrital zircon U-Pb, TE, Lu-Hf; CA-TIMS; ID-TIMS; LA-ICP-MS, ⁴⁰Ar/³⁹Ar hornblende, muscovite, biotite

1. Introduction

In 2018, the British Columbia Geological Survey initiated a three-year mapping project in the Omineca Mountains of north-central British Columbia (Figs. 1, 2; Ootes et al., 2019, 2020a,b). The project aims to better understand the geology and associated base- and precious-metal mineralization in the northern part of Hogem batholith and adjacent supracrustal rocks of the Quesnel, Stikine, and Cache Creek terranes.

Herein we present analytical results from samples collected during bedrock mapping in 2018 and 2019. This includes data from whole rock geochemical analysis, whole rock Nd and Sr isotope analysis, U-Pb zircon igneous crystallization data from chemical abrasion isotope dilution thermal ionization mass-spectrometry (CA-TIMS), and laser ablation inductively coupled plasma mass-spectrometry (LA-ICP-MS), ⁴⁰Ar/³⁹Ar (hornblende, muscovite, and biotite) step-heating results, and LA-ICP-MS detrital zircon U-Pb, Lu-Hf, and trace element data. The whole rock geochemical data, U-Pb igneous zircon crystallization ages, and ⁴⁰Ar/³⁹Ar ages for the northern Hogem batholith samples support the results presented in Jones et al. (2021). Graphed results and interpretations of two CA-TIMS and three ⁴⁰Ar/³⁹Ar step heating analyses were presented in

Ootes et al. (2020b). The data in this GeoFile also include legacy U-Pb zircon crystallization ages determined by ID-TIMS from bedrock samples north of Hogem batholith that were released by Schiarizza and Tan (2005) without supporting data.

This GeoFile serves as a data repository for summaries and interpretations presented by Ootes et al., (2020a,b), Jones et al. (2021), and forthcoming studies. Five appendices are included ([BCGS_GF2020-01.zip](#)). Appendix 1 includes a table of bedrock units and their salient features (Table 1) and a table of samples, locations, and analytical work completed on each (Table 2). Appendix 2 contains assay results, whole rock major and trace element geochemical results, and Rb-Sr and Sm-Nd isotopic results from samples collected during bedrock mapping. Appendix 3 contains new U-Pb crystallization results and supporting data, determined from CA-TIMS, LA-ICP-MS, and ID-TIMS (mechanical abrasion, multi-grain analyses). For samples analyzed by LA-ICP-MS, images of zircon grain mounts with beam-spot locations are included (mainly cathodoluminescence, CL, two examples by electron backscatter BS). Appendix 4 contains results from ⁴⁰Ar/³⁹Ar laser step heating. Appendix 5 contains the results of detrital zircon U-Pb, trace element, and Lu-Hf isotopic results. Zircon

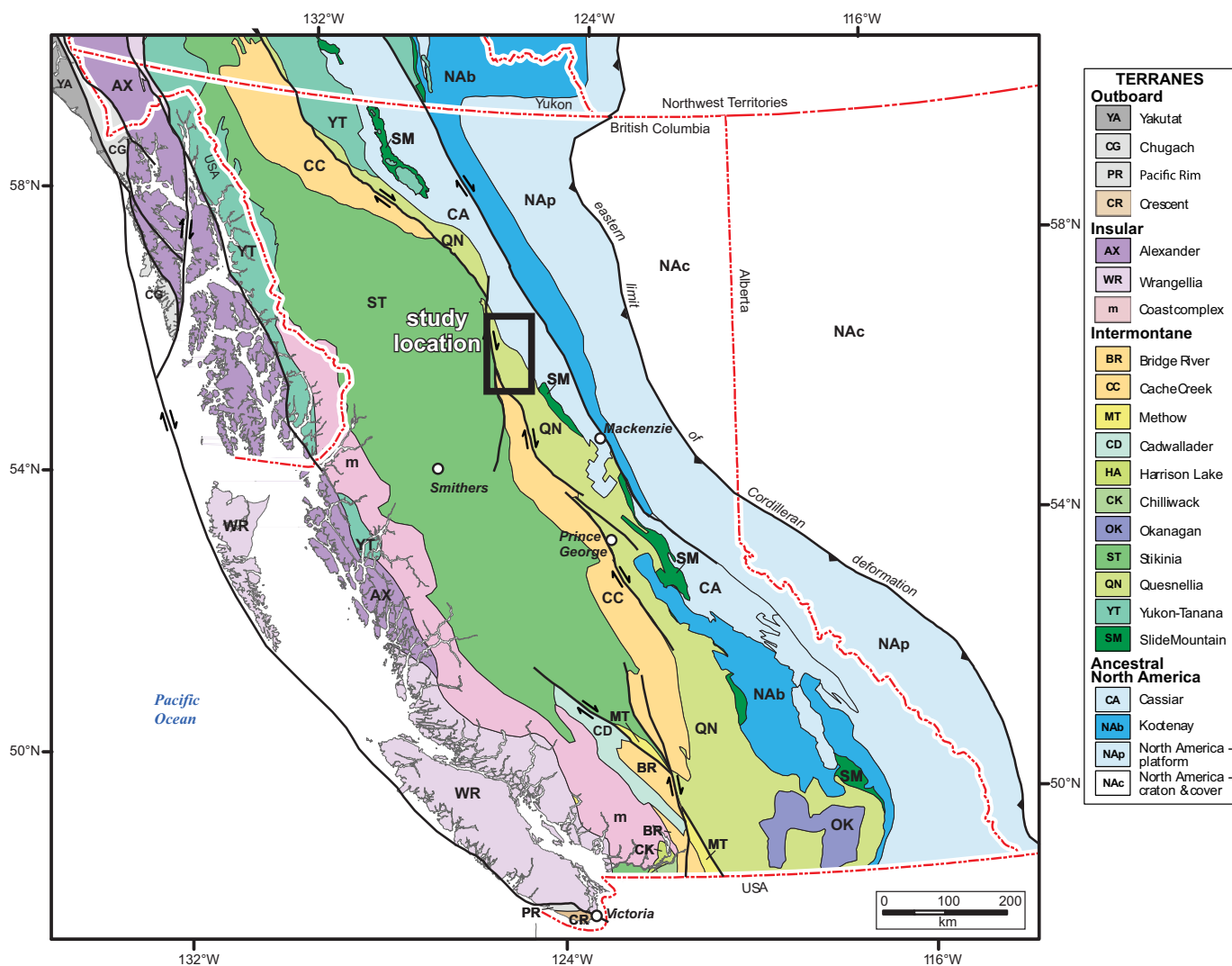


Fig. 1. Location of Hogem batholith study area with respect to Cordilleran terranes of British Columbia. Modified after Nelson et al. (2013).

cathodoluminescence (CL) images for detrital zircon grain mounts for each sample are in Appendix 5.

2. Geology

The Hogem batholith is in the Quesnel terrane and intrudes supracrustal rocks of the Nicola Group (Figs. 1, 2; Schiarizza and Tan, 2005; Ootes et al., 2020a). Herein we use the term Nicola Group for these supracrustal rocks to be consistent with equivalent rocks elsewhere in the Quesnel terrane and to avoid confusion with the Takla Group in the neighbouring Stikine terrane such as mapped, for example, by Monger (1977). The intrusive units in Hogem batholith are assigned to the Thane Creek, Duckling Creek, Osilinka, and Mesilinka suites and each contain a family of igneous compositions (Tables 1, 2; Appendix 1). In general, we assign each suite based on its rock type, supported with whole rock geochemistry (Appendix 2) and U-Pb zircon crystallization ages (Appendix 3, 4; Jones et al., 2021). Geophysical attributes from a recent magnetic-radiometric geophysical survey (CGG Canada Services Ltd., 2018) have also been used (Table 1).

The Quesnel terrane is separated from the Cache Creek and Stikine terrane by the dextral strike-slip Pinchi-Ingenika fault (Figs. 1, 2). In the study area, the Stikine terrane includes the Asitka Group (Stikine assemblage), the Dewar Formation (Takla Group) and the Telka Formation (Hazelton Group). This study presents the results of detrital zircon U-Pb, Lu-Hf, and trace elements for samples from the Asitka Group and the Telkwa Formation (Appendix 5). Stikine and Cache Creek terranes are in contact along a thrust fault (Fig. 2; Ootes et al., 2020a), where the Cache Creek terrane is interpreted to have been thrust over Stikine terrane rocks. The Sitlika assemblage is a suite of mixed volcanic and sedimentary rocks that overlap Cache Creek and Stikine terrane rocks. This study presents the results of detrital zircon U-Pb, Lu-Hf, and trace elements for a sample from the Sitlika assemblage (Appendix 5).

3. Whole-rock geochemistry

3.1. Major, trace, and rare earth element geochemistry

Samples for whole rock geochemistry were collected during bedrock mapping in 2018 and 2019. In the field, alteration

and lichen-free samples were prepared as chips, bagged, and sealed. Typically, we collected fist-size samples but larger samples were collected for coarser-grained rocks, or rocks with phenocrysts. Where samples could not be cleaned in the field, weathering surfaces were removed using a rock saw, then thoroughly washed and dried. Sampling was conducted by L. Ootes, D. Milidragovic, A. Bergen, B. Graham, and G. Jones. Samples with the abbreviation 03PSC and 04PSC were collected by P. Schiarizza and were extracted from the British Columbia Geological Survey archives.

Prepared samples were submitted to Actlabs. Ancaster, Ontario, for whole rock major, trace, and rare earth element analysis. At Actlabs, samples were crushed to pass 2 mm, mechanically split using a rifle splitter, and pulverized using mild steel to 95% passing 105 μm (Code RX-2). Lithium metaborate/tetraborate fusion was performed on the resulting pulp to produce a molten bead, which was rapidly digested in nitric acid solution. Major element oxides were determined using inductively coupled plasma optical emission spectroscopy (ICP-OES) and trace element concentrations were determined using inductively coupled plasma mass spectrometry (ICP-MS; Code 4 Lithoresearch). Measurement accuracy was determined using certified standards provided by Actlabs. In addition, in 2018 three blind samples of the British Columbia Geological Survey in-house till standard (BCGS Till 2013) were analyzed and in 2019 the certified reference samples SY-4, GSP-2, and TDB-1 were analyzed with the unknowns. Duplicate samples were run every 10-20 measurements.

Major element accuracy is within 5% error and precision better than 5% relative standard deviation (RSD), typically better than 2% RSD. Major element concentrations that have greater than 5% error are in low concentration (<1 wt. %). Minor and trace element accuracy is within 10% error and typically the higher error is associated with elements with low concentrations (<10 ppm). The rare earth elements (REEs) were determined to be within 10% of the accepted standard values. Minor and trace element precision was generally 5% RSD or better. Duplicate measurements with RSD higher than 10% were more common in the 2018 analysis than 2019. Results are in Appendix 2 (Tables “Hogem_geochem_18” and “Hogem_geochem_19”).

3.2. Rb-Sr and Sm-Nd

Samples from each of the intrusive suites were selected for radiogenic isotope analysis. All have corresponding major and trace element geochemistry, and most have accompanying U-Pb zircon and/or $^{40}\text{Ar}/^{39}\text{Ar}$ data (Table 2; Appendix 1). Sample powders were prepared by creating cm-sized chips in a jaw crusher then reducing to a powder by hand-milling with an agate mortar and pestle. Powdered samples were sent to the Isotope Geochronology and Geochemistry Research Centre (IGGRC), Carleton University, Ottawa, ON, where they were prepared in a clean lab. The Sr and Nd isotope ratios were measured using two Thermo-Finnigan mass spectrometers, a Neptune multi-collector (MC)-ICP-MS, and a Triton thermal ionization mass spectrometer (TIMS). Between 50 and 150 milligrams were dissolved in a mixture of concentrated HF and HNO_3 on the hotplate at 130°C for 72 hours before they were evaporated to dryness; the residues were then re-dissolved in 7M HNO_3 and 6M HCl. Strontium and Nd were sequentially

separated following the ion exchange column procedures described in Cousins (1996), except that Nd was separated using the pre-slurry-packed 2ml LN-resin columns (Eichrom Technologies LLC, USA). In addition, a Sr-Spec resin (Eichrom Technologies, LLC, USA) column procedure was used to clean the Sr fractions for those measured on the Neptune MC-ICP-MS. Columns were washed with 16 ml of 2.5 M HCl before Sr fractions were collected in 7 ml 2.5 M HCl; the columns were washed in 3.5 ml of 6M HCl before REE were eluted using 9 ml of 6M HCl. Rare earth element fractions were dissolved in 0.26M HCl and loaded onto Eichrom Ln Resin 2ml prepacked (slurry packed) chromatographic columns containing Teflon powder coated with HDEHP [di(2-ethylhexyl) orthophosphoric acid (Richard et al., 1976). Neodymium was eluted using 0.26M HCl. Strontium fractions were cleaned using the Sr spec resin before measurement on the Neptune MC-ICP-MS.

Strontium isotopic ratios were normalized to $^{86}\text{Sr}/^{88}\text{Sr}=0.1194$ and Nd isotopic ratios normalized to $^{146}\text{Nd}/^{144}\text{Nd}=0.7219$. The $^{143}\text{Nd}/^{144}\text{Nd}$ measured by the Neptune MC-ICP-MS were further normalized for the offsets using the bracketing JNdi-1 average values against an IGGRC's Triton JNdi-1 average value of 0.512100.

The results for the routine measurements of bracketing standard reference materials during a period between six and eighteen months are summarized as follows. Measurements of NBS987 and USGS standard BCR-2 with the Neptune MC-ICP-MS and Triton TIMS yield average $^{87}\text{Sr}/^{86}\text{Sr}$ ratios, 0.710250 ± 0.000020 (2SD, n=29) and 0.705009 ± 0.000053 (2SD, n=7), and 0.710240 ± 0.000018 (2SD, n=26) and 0.704998 ± 0.000018 (2SD, n=6), respectively; measured by the Neptune MC-ICP-MS, the average $^{143}\text{Nd}/^{144}\text{Nd}$ ratios of international standard JNdi-1 (Tanaka et al, 2000) and BCR-2 are 0.512086 ± 0.000011 (2SD, n=44) and 0.512626 ± 0.000006 (2SD, n=4), respectively; the latter is within the uncertainty identical to BCR-2's average $^{143}\text{Nd}/^{144}\text{Nd}$ value of 0.512623 ± 0.000011 (n=7, 2SD) measured by Triton TIMS; routinely measuring a Nd metal in-house standard with the Triton TIMS gives an average $^{143}\text{Nd}/^{144}\text{Nd}$ value of 0.511814 ± 0.000009 (2SD, n=21), an equivalent value of 0.512100 for JNdi-1. Average $^{143}\text{Nd}/^{144}\text{Nd}$ and $^{87}\text{Sr}/^{86}\text{Sr}$ values of BHVO-2 are 0.512970 (n=2) and 0.703485 (n=2) by the Neptune MC-ICP-MS, comparable within the uncertainty to the values of 0.512963 (n=1) and 0.703475 (n=2) by the Triton TIMS. The total procedure blanks in IGGRC lab are <250pg for Sr and <50 pg for Nd.

Sample powders were prepared at the BCGS by L. Ootes. At Carleton University, S. Zhang conducted the analytical work. Results are in Appendix 2 (Table “Hogem_Sr-Nd_isotopes”).

3.3. Assay data

Samples for assay were collected as grab samples from outcrops with identifiable or indicative metallic mineralization (e.g., malachite staining). Samples were sent to Activation Laboratories (Ancaster, Ontario) where they were crushed and pulped using mild steel (Code RX-1) and analyzed by a combination of instrumental neutron activation analysis (INAA) and acid dilution ICP-MS (Code 1H). Two samples from 2018 contained Cu values above detection limit of 10,000 ppm and were further analyzed by acid dilution inductively coupled plasma optical emission spectrometry (ICP-OES). Assay results with elemental values that correspond to known

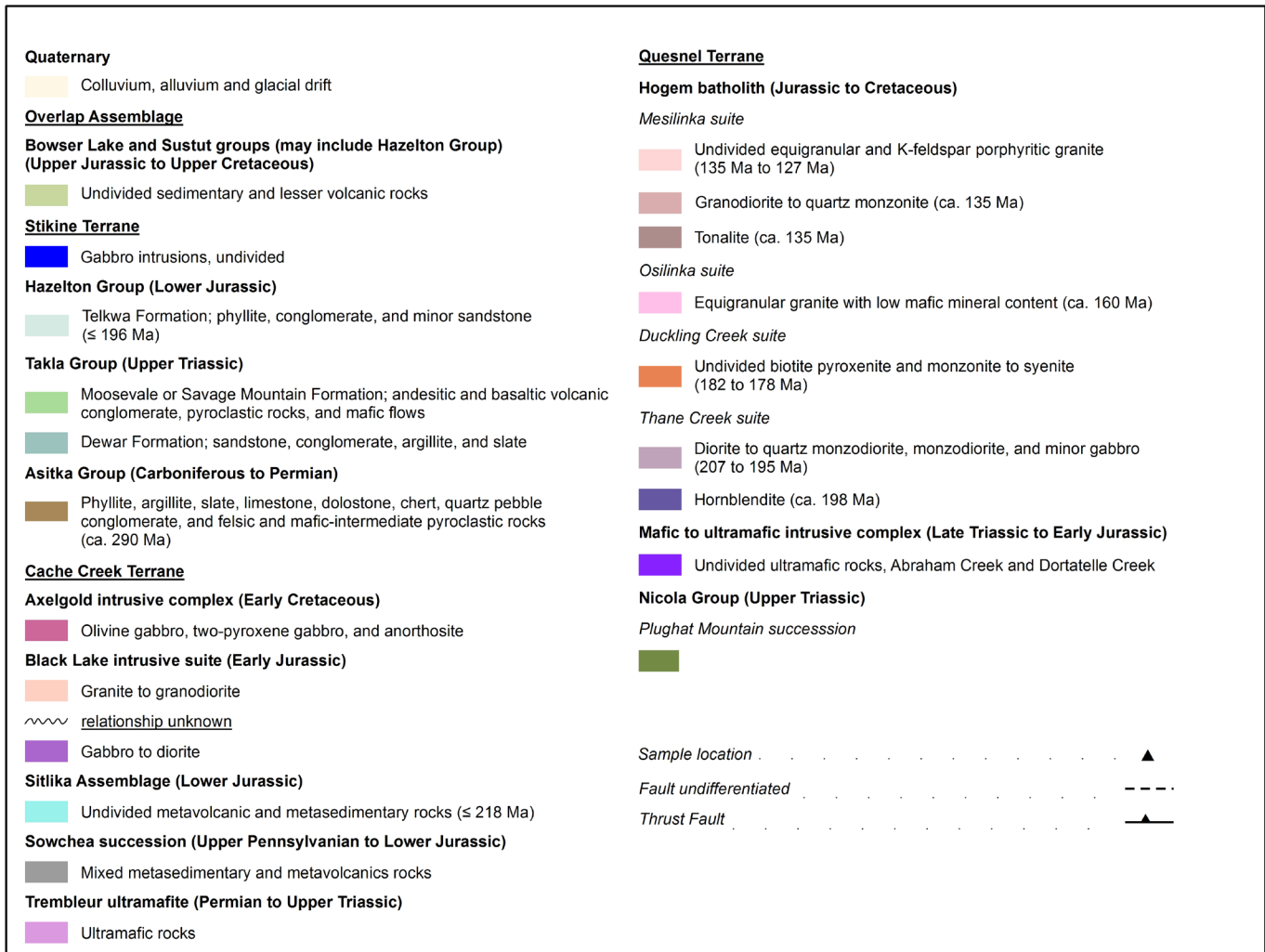


Fig. 2. continued.

Scoates and Friedman (2008). After rock samples underwent standard mineral separation procedures, zircons were handpicked in alcohol. The clearest, crack- and inclusion-free grains were selected, photographed, and then annealed in quartz glass crucibles at 900°C for 60 hours. Annealed grains were transferred into 3.5 mL PFA screwtop beakers; ultrapure HF (up to 50% strength, 500 mL) and HNO₃ (up to 14N, 50 mL) were added and caps closed finger tight. The beakers were placed in 125 mL PTFE liners (up to four per liner) and about 2 mL HF and 0.2 mL HNO₃ of the same strength as acid within beakers containing samples were added to the liners. The liners were slid into stainless steel Parr™ high pressure dissolution devices, sealed and brought up to a maximum of 200°C for 8-16 hours (typically 175°C for 12 hours). Beakers were removed from liners and zircon separated from leachate. Zircons were rinsed with >18 MΩ.cm water and subboiled acetone. Then 2 mL of subboiled 6N HCl was added and beakers set on a hotplate at 80°-130°C for 30 minutes and again rinsed with water and acetone. Masses were estimated from the dimensions (volumes) of grains and single grains were transferred into clean 300 mL PFA microcapsules (crucibles), and 50 mL 50% HF and 5 mL 14N HNO₃ added. Each was spiked with a ²³³⁻²³⁵U-²⁰⁵Pb

tracer solution (EARTHTIME ET535), capped and placed in a Parr™ liner (8-15 microcapsules per liner). To the liner, HF and nitric acids were added in a 10:1 ratio and then placed in Parr™ high pressure device and dissolution was achieved at 220°C for 40 hours. The resulting solutions were dried on a hotplate at 130°C, 50 mL 6N HCl was added to microcapsules and fluorides were dissolved in high pressure Parr™ devices for 12 hours at 180°C. The HCl solutions were transferred into clean 7 mL PFA beakers and dried with 2 mL of 0.5N H₃PO₄. Samples were loaded onto degassed, zone-refined Re filaments in 2 mL of silicic acid emitter (Gerstenberger and Haase, 1997). Isotopic ratios were measured with a single collector VG 54R thermal ionization mass spectrometer equipped with analogue Daly photomultiplier. Analytical blanks are 0.1 pg for U and up to 1.5 pg for Pb. Uranium fractionation was determined directly on individual runs using the EARTHTIME ET535 mixed ²³³⁻²³⁵U-²⁰⁵Pb isotopic tracer (Schmitz and Schoene, 2007) and Pb isotopic ratios were corrected for fractionation of 0.25 ± 0.04%/amu, based on replicate analyses of NBS-982 reference material and the values recommended by Thirlwall (2000). Data reduction employed the Excel-based program of Schmitz and Schoene (2007). Standard concordia diagrams were constructed

Table 1. Lithostratigraphic summary, unit geophysical attributes, and summaries of Sm-Nd and Rb-Sr results and U-Pb ages.

Terrane	Group or intrusive suite	Formation or sub unit	Characteristic	Deformation
Post-accretionary	Mesilinka	equigranular granite	bioite granite +/- garnet, muscovite	yes - foliation (biotite)
		K-feldspar porphyritic granite	biotite granite with K-feldspar phenocrysts	yes - foliation (biotite)
		granodiorite	equigranular biotite annd hornblende-bearing	yes - foliation (biotite)
		tonalite	grey equigranular enclaves in younger granite	yes - foliation (biotite)
Osilinka	dykes, sills	felsic and mafic hypabyssal porphyry	yes - weak to mylonitic	
	equigranular granite	low mafic minerals (<5%) +/- garnet, muscovite	yes -weak foliation (biotite) - crossing dykes locally mylonitized	
Quesnel	Duckling Creek	syenite to monzonite	equigranular to K-feldspar porphyritic; local well-developed igneous layering	yes - weak (feldspar)
		biotite pyroxenite	pyroxenite, with biotite, local apatite phenocrysts	yes - locally strong (biotite-pyroxene)
	Thane Creek	monzodiorite to quartz monzodiorite	quartz bearing diorite	yes - polyphase (two generaltions of fabric development)
		diorite	equigranular medium to coarse-grained; commonly contains hornblendite enclaves; locally altered with epidote and biotite common	yes - polyphase (two generaltions of fabric development)
		hornblendite	coarse grained to pegmatitic; local coarse plagioclase segregations; intermingled with diorite	recrystallized amphibole
	Mafic-ultramafic intrusions	unnamed	olivineand clinopyroxene-rich ultramafic rock types	sheared margins
Abraham Creek		hornblende gabbro, diorite, and clinopyroxenite with lesser peridotite, hornblendite, and orthopyroxenite		
Nicola Group	Plughat Mountain succession	augite-plagioclase phyric mafic tuffs and volcanic breccias with lesser volcanic flows, tuffaceous sedimentary rocks, argillite, and limestone	yes - polyphase	
Cache Creek	Sitlika	schist	yes - polyphase	
Stikine	Hazelton Group	Telkwa Formation	polymictic and monomictic volcaniclastic conglomerates; interleaved red/green weathered	yes - polyphase (two generations of fabric development)
	Takla Group	Dewar Formation	mafic-volcanic-derived sandstone, pebble and boulder polymictic conglomerate, and slate	yes - polyphase (two generations of fabric development)
	Asitka Group		phyllite, carbonate beds, chert, lesser rhyolite and basaltic andesite, and rare quartz pebble sandstone	yes - polyphase (two and possibly three generations of fabric development)

*CGG Canada Servies, Ltd. (2018) geophysical survey: Hogem batholith interpretation only

^bt =biotite; hbl=hornblende; mv=muscovite

^^ Estimated maximum dpeosition age

Table 1. continued.

Group or intrusive suite	*Geophysical attribute	Whole rock geochemistry	Whole rock ϵ Nd(t)	Whole rock Sr/Sr(i)	U-Pb age (Ma) (CA-TIMS)	U-Pb age (Ma) (TIMS)	U-Pb age (Ma) (LA-ICP-MS)
Mesilinka	low mag, high Th/K	yes	3.3	0.703479		133.9±0.3	127.9±0.8
	low mag, high Th/K	yes	1.7	0.704000		135.0±0.3	134.8±1.2
	low mag	yes					
	low mag	yes					134.1±0.5
Osilinka	-	yes					inherited zircon to ca. 160
	low mag, low Th/K	yes	4.1	0.703726			inherited zircon to ca. 160
Duckling Creek	high mag, low Th/K	yes	4.7	0.703678			174.7±0.7 178.9±1.3
	very high mag, low Th/K	yes					
Thane Creek	variable mag, moderate Th/K	yes	4.8	0.703548			194.0±1.1
	variable mag, moderate Th/K	yes	4.8	0.703665	196.6±0.9		206.6±0.9
	high mag; low radiometric signature	yes			197.6±0.1		191.4±0.7
Mafic-ultramafic intrusions	high mag; low radiometric signature				216.8±0.2	219.6±0.3	
Nicola Group		yes					
Sitlika							
Hazelton Group							
Takla Group							
Asitka Group		yes			288.6±0.2 293.9±0.3		

Table 1. continued.

Group or intrusive suite	Ar-Ar [^]	Detrital zircon U-Pb (Ma) ^{^^}	Detrital zircon Hf
Mesilinka	bt - 112±3 hbl bt - 123±2 bt - 108±2 bt - 111±3		
Osilinka	mv - 122±5 bt - 116 ±1		
Duckling Creek	hbl - 177±5		
Thane Creek	hbl - 202±5 hbl - 124±2 bt - 124±1 bt - 126±2		
Mafic-ultramafic intrusions			
Nicola Group			
Sitlika		<218	x
Hazelton Group		<196	x
Takla Group		no zircon	
Asitka Group		<323	x

and regression intercepts and weighted averages calculated with Isoplot (Ludwig, 2003). Unless otherwise noted all errors are quoted at the 2 sigma, or 95% level of confidence. Isotopic dates are calculated with the decay constants $\lambda_{238} = 1.55125E-10$ and $\lambda_{235} = 9.8485E-10$ (Jaffey et al., 1971) and a $^{238}\text{U}/^{235}\text{U}$ ratio of 137.88. EARTHTIME U-Pb synthetic solutions were analyzed on an on-going basis to monitor the accuracy of results.

Sampling was conducted by L. Ootes and D. Milidragovic. At PCIGR, R. Friedman oversaw zircon separation and analyses. Results are in Appendix 3 (Tables “CA-TIMS_ThaneCk” and “CA-TIMS_Asitka”).

4.1.1. Abraham Creek diorite-gabbro: DMI19-25-1

The sample is from the Abraham Creek intrusive complex, 17.8 km northeast of Horn Peak. It is from a unit of heterogeneous, epidote-altered hornblende-clinopyroxene diorite-gabbro, devoid of clinopyroxenite enclaves. A clinopyroxenite unit locally cuts this unit; near the contact, gabbro-diorite forms a magmatic breccia with abundant angular clinopyroxenite fragments in a dioritic groundmass (see figure 4b in Ootes et al., 2020b). The sample is coarse-grained hornblende diorite (lacking clinopyroxene). Plagioclase is completely altered to saussurite and epidote. Amphibole is partly altered to chlorite. Accessory apatite and titanite (titanite as inclusions in amphibole) make up 3-5 % of rock. Approximately 5% of the sample is magnetite.

Five zircons yield a tight spread of concordant ages from 217.8 to 216.8 Ma. Three older zircons may be antecrysts (or potentially xenocrysts) and the two youngest overlapping zircons have a $^{206}\text{Pb}/^{238}\text{U}$ weighted mean age of 216.8 ± 0.2 Ma, interpreted as the time of crystallization. ID-TIMS results of multi-zircon fractions from an equigranular diorite collected near the northwest end of the complex yield an age of 219.6 ± 0.3 Ma (see section 4.2.2).

4.1.2. Thane Creek hornblende: 18lo22-1a

The sample is from the Thane Creek suite, 18.6 km south-southeast of Mount Ferris. The sample is a coarse-grained to pegmatitic plagioclase-bearing hornblende. Pegmatitic white hornblende-plagioclase segregations are interstitial to predominantly green hornblende. Hornblende is commonly overgrown by brown or green biotite, with biotite making up ~10% of the sample. The sample contains ~5% magnetite that is interstitial to amphibole and is concentrated with accessory titanite and apatite. Coarse, subhedral accessory epidote occurs in pegmatitic plagioclase segregations. Trace fine-grained chalcopyrite is disseminated through the sample.

Four zircons yield a tight overlap of concordant ages with a $^{206}\text{Pb}/^{238}\text{U}$ weighted mean age of 197.6 ± 0.1 Ma, interpreted as the crystallization age.

4.1.3. Thane Creek diorite: 18lo22-1d

The sample is from the Thane Creek suite, 18.6 km south-southeast of Mount Ferris. It consists of medium-grained equigranular diorite and is also dated by $^{40}\text{Ar}/^{39}\text{Ar}$ hornblende and biotite (section 5.1.1). The rock is deformed and contains a moderate foliation defined by plagioclase and biotite and amphibole. The sample is mostly clay-altered plagioclase (65%), biotite (12%), and amphibole (6%). Minor altered alkali feldspar (7%) and quartz (1-2%) are present, interstitial

Table 2. Units sampled, sample numbers, locations, rock types, and analyses performed.

Unit	Sample#	Alias	Rock type	Lat	Long
Darb Lake pluton	03PCS-295	PCS03-295	tonalite	56.5165	-126.1168
Abraham Creek	03PCS-296	PCS03-296	diorite	56.4577	-126.0259
Solo Lake stock	03PSC-298	PCS03-298	diorite	56.5335	-126.2428
	04PSC-330	PCS04-330	diorite	56.5559	-126.1377
Johanson Lake stock	04PSC-329	PCS04-329	monzonite	56.5896	-126.1576
Johanson Creek	04PSC-327	PCS04-327	tonalite	56.6085	-126.3053
Davie Creek stock	03PSC-297	PCS03-297	granite	56.4571	-126.0117
Mesilinka	04PSC-277	PCS04-277	equigranular granite	56.3892	-126.0589
Mesilinka	04PSC-278	PCS04-278	porphyritic granite	56.3905	-126.0757
Mesilinka	18lo11-1	LOO18-11-1	equigranular granite	56.221037	-125.932380
Mesilinka	18lo12-7	LOO18-12-7	porphyritic granite	56.223797	-125.923148
Mesilinka	18bg17-10	BGR18-17-10	tonalite	56.091248	-125.947834
Mesilinka	19GJ12-1	GJO19-12-1	tonalite	56.223775	-125.974787
Mesilinka	18lo19-2	LOO18-19-2	granodiorite	56.068745	-125.988290
Osilinka sheet	18lo20-4	LOO18-20-4	felsic porphyry	56.100984	-125.732593
Osilinka	18lo17-1	LOO18-17-1	granite	56.110442	-125.764089
Osilinka	18ab5-6	ABE18-5-6	granite	56.167982	-125.810132
Duckling Creek	18lo25-2a	LOO18-25-2a	syenite	56.007961	-125.701574
Duckling Creek	18lo24-1	LOO18-24-1	syenite	56.012295	-125.681727
Duckling Creek	19GJ13-5a	GJO19-13-5a	syenite	55.999451	-125.526168
Thane Creek	19GJ12-4	GJO19-12-4	diorite	56.211666	-125.646053
Thane Creek	19GJ13-3	GJO19-13-3	quartz monzodiorite	56.024407	-125.598711
Thane Creek	18lo26-1	LOO18-26-1	quartz monzodiorite	56.057991	-125.607348
Thane Creek	18lo22-1d	LOO18-22-1d	diorite	56.013314	-125.820707
Thane Creek	18lo22-1a	LOO18-22-1a	hornblende	56.013314	-125.820707
Abraham Creek	DMI19-25-1	DMI19-25-1	diorite-gabbro	56.344995	-125.777827
Asitka Group	19lo5-5	LOO19-5-5	fragmental rhyolite	56.287230	-126.229131
Asitka Group	19lo7-3d	LOO19-7-3d	rhyolite	56.402956	-126.296428
Asitka Group	19lo14-5	LOO19-14-5	quartz pebble sandstone	56.244247	-126.384625
Sitlika Assemblage	DMI19-9-12	DMI19-9-12	feldspathic sandstone	55.991	-126.116167
Telkwa Formation	19GJ18-3	GJO19-18-3	feldspathic sandstone	56.227279	-126.25884

*only samples with data other than whole rock geochemistry are included in this table

^University of Alberta; ^^University of British Columbia

z=zircon; t=titanite; bt=biotite; hbl=hornblende; mv=muscovite

to plagioclase. Accessory anhedral to subhedral, fine-grained epidote, apatite, and magnetite occur with biotite. Trace fine-grained chalcopyrite is disseminated through the sample. Four zircons yield a spread of concordant ages from 198.8 to 196.6 Ma. The three older zircons are interpreted as antecrysts, and the youngest zircon has a $^{206}\text{Pb}/^{238}\text{U}$ date of 196.6 ± 0.9 Ma, interpreted as the maximum age for crystallization.

4.1.4. Asitka Group rhyolite: 19lo5-5

The sample, from the Asitka Group 8.8 km northeast of Mount Carruthers, is of red and green weathering fragmental rhyolite with heterogeneous volcanic clasts up to 10 cm. The rocks are moderately to strongly deformed, with a foliation defined by a groundmass cleavage and clast alignment. Four of five zircons yield a tight overlap on concordia at ca. 294 Ma. The fifth zircon overlaps concordia at ca. 290 Ma and is interpreted to have had Pb-loss. The four overlapping concordant ages yield a $^{206}\text{Pb}/^{238}\text{U}$ weighted mean of 293.9 ± 0.3 Ma, interpreted as the

crystallization age of the fragmental rhyolite.

4.1.5. Asitka Group rhyolite: 19lo7-3d

The sample is from the Asitka Group, 4.4 km southwest of Doratelle Peak. It is from a 30 cm thick, fine-grained rhyolite that is interbedded with 2 m thick basaltic andesite and is 5 m below red chert, a potential marker horizon within the Asitka Group. The stratigraphic relationship of the volcanic rocks and chert is uncertain because younging directions are not preserved at this location. Six concordant zircons yield a tight overlap on concordia, with $^{206}\text{Pb}/^{238}\text{U}$ weighted mean age of 288.6 ± 0.2 Ma, interpreted as the time of crystallization.

4.2. ID-TIMS

The analytical techniques in this section refer to samples collected for U-Pb geochronology near the very northern part of Hagem batholith and farther north. The main difference between these analyses and the CA-TIMS is that the zircons

Table 2. continued.

Sample#	Igneous						Detrital		
	whole rock		mineral				mineral		
	*geochemistry	Sr-Nd	CA-TIMS	TIMS	LA-ICPMS [^]	Ar-Ar	LA-ICPMS ^{^^}	TE	Hf
03PCS-295				z					
03PCS-296				z					
03PSC-298	x			z					
04PSC-330	x			z					
04PSC-329	x			z					
04PSC-327				z, t					
03PSC-297	x			z					
04PSC-277				z, t					
04PSC-278	x			z, t					
18lo11-1	x	x			z				
18lo12-7	x	x			z	bt			
18bg17-10	x					bt			
19GJ12-1	x				z				
18lo19-2	x					hbl, bt			
18lo20-4					z				
18lo17-1	x				z	bt, mv			
18ab5-6		x				no result			
18lo25-2a		x			z				
18lo24-1						hbl			
19GJ13-5a	x				z				
19GJ12-4	x				z				
19GJ13-3	x				z				
18lo26-1	x	x				hbl			
18lo22-1d	x	x				hbl, bt			
18lo22-1a	x			z	z				
DMI19-25-1	x			z					
19lo5-5				z					
19lo7-3d				z					
19lo14-5							z	z	z
DMI19-9-12							z	z	z
19GJ18-3							z	z	z

received a mechanical air abrasion treatment rather than chemical abrasion (section 4.1.). In addition, all but one of the zircon results are multi-grain instead of single grain analyses. All sample preparation, geochemical separations, and mass spectrometry were completed at the PCIGR. Zircon and titanite were separated from samples using conventional crushing, grinding, and Wilfley table techniques, followed by final concentration using heavy liquids and magnetic separations. Mineral fractions for analysis were selected on the basis of grain quality, size, magnetic susceptibility, and morphology. All zircon fractions were air abraded before dissolution to minimize the effects of post-crystallization Pb-loss, using the technique of Krogh (1982).

Zircons were dissolved in sub-boiled 48% HF and 16 M HNO₃ (ratio of ~10:1, respectively) in the presence of a mixed ²³³⁻²³⁵U-²⁰⁵Pb tracer; zircons for 40 hours at 240°C in 300 mL PTFE and PFA microcapsules contained in high pressure vessels (Parr™ acid digestion vessels with 125 mL PTFE liners), and titanites on a hotplate in 7 mL screwtop PFA beakers for at least 48 hours at ~130°C. Sample solutions were then dried to salts at ~130°C. Zircon residues were re-dissolved in ~200 mL

of sub-boiled 3.1N HCl for 12 hours at 210°C in high pressure vessels and titanite residues on a hotplate in 1 mL of sub-boiled 6.2N HCl in 7 mL screwtop PFA beakers for at least 24 hours at ~130°C. Titanite solutions were again dried to salts and were again re-dissolved on a hotplate, in the same beakers, in 1 mL of sub-boiled 3.1N HCl at ~130°C for at least 24 hours. Separation and purification of Pb and U employed ion exchange column techniques modified slightly from those described by Parrish et al. (1987). Lead and U were sequentially eluted into a single beaker; U from titanite solutions was purified by passing through columns a second time. Elutants were dried in 7 mL screwtop PFA beakers on a hotplate at ~120°C in the presence of 2 mL of ultrapure 1N H₃PO₄. Samples were then loaded on single, degassed zone refined Re filaments in 5 mL of a silica gel (SiCl₄) phosphoric acid emitter. Isotopic ratios were measured using a modified single collector VG-54R thermal ionization mass spectrometer equipped with an analogue Daly photomultiplier. Measurements were done in peak-switching mode on the Daly detector. Uranium and Pb analytical blanks were in the range of 1 pg or less and 2-5 pg (both ± 50%), respectively, during the course of this

study. Uranium fractionation was determined directly on individual runs using the $^{233-235}\text{U}$ tracer, and Pb isotopic ratios were corrected for fractionation of $0.37\%/amu \pm 0.05\%/amu$, based on replicate analyses of the NBS-981 Pb standard and the values recommended by Thirlwall (2000). Data reduction employed the Excel-based program of Schmitz and Schoene (2007). Standard concordia diagrams were constructed and regression intercepts and weighted averages calculated with Isoplot (Ludwig, 2003). Unless otherwise noted all errors are quoted at the 2 sigma or 95% level of confidence. Isotopic dates were calculated with the decay constants $\lambda_{238}=1.55125\text{E-}10$ and $\lambda_{235}=9.8485\text{E-}10$ (Jaffe et al., 1971) and a $^{238}\text{U}/^{235}\text{U}$ ratio of 137.88.

Samples were collected by P. Schiarizza. At PCIGR, R. Friedman oversaw the sample processing and analytical procedures. The original data was re-reduced in 2020 using the program of Schmitz and Schoene (2007). Results are in Appendix 3 (Table "TIMS_PSC03_04").

4.2.1. Darb Creek pluton: 03PSC-295

The Darb Creek pluton comprises tonalite that cuts the Nicola Group 12 km north of the Hogem batholith (8.5 km south of Johanson Lake). The sample is medium-grained equigranular hornblende-biotite tonalite collected from the south margin of the pluton, 7.2 km south-southeast of Johanson Lake.

Two zircon fractions yield concordant results and a weighted mean $^{206}\text{Pb}/^{238}\text{U}$ date of 177.3 ± 0.4 Ma (MSWD=0.48), interpreted as the time of crystallization. Two significantly older results run up concordia, likely due to some xenocrystic grains and/or grains with xenocrystic cores. One result, near the young end of titanite data, likely reflects Pb-loss. The oldest of three multi-grain titanite fractions yields a $^{206}\text{Pb}/^{238}\text{U}$ date of 174.2 ± 0.6 Ma. The titanite ages young as a function of diminishing grain size.

4.2.2. Abraham Creek intrusive complex: 03PSC-296

The Abraham Creek intrusive complex, including diorite, gabbro, hornblendite, clinopyroxenite and intrusion breccia, forms a markedly elongate, northwest-trending body that cuts the Nicola Group northeast of the Hogem batholith. The sample is medium-grained equigranular diorite collected near the northwest end of the complex, 17 km southeast of Johanson Lake.

Two multi-grain zircon fractions yield overlapping Concordia ages with a weighted mean $^{206}\text{Pb}/^{238}\text{U}$ date of 219.6 ± 0.3 Ma (MSWD=0.73). Two other fractions are discordant and are interpreted to have had Pb-loss.

4.2.3. Davie Creek stock: 03PSC-297

The Davie Creek granitic stock, about 700 m by 300 m, cuts clinopyroxenite and related rocks near the northwest end of the Abraham Creek intrusive complex, and hosts the Davie Creek porphyry molybdenum prospect. The sample is a medium-grained equigranular biotite granite from the northern part of the stock, 16.7 km southeast of Johanson Lake.

Three multi-grain zircon fractions yield overlapping concordia ages with a weighted mean $^{206}\text{Pb}/^{238}\text{U}$ date of 136.6 ± 0.2 Ma (MSWD=2.0). One older fraction is interpreted as inherited and one younger fraction is interpreted to record Pb-loss.

4.2.4. Solo Lake stock: 03PSC-298A

The Solo Lake stock is a small diorite to quartz diorite intrusion that cuts the Nicola Group 7 km southwest of Johanson Lake. The sample is medium-grained equigranular hornblende diorite collected near the north margin of the stock, 6.8 km southwest of Solo Lake.

Three multi-grain zircon fractions yield overlapping concordia ages with a weighted mean $^{206}\text{Pb}/^{238}\text{U}$ date of 223.7 ± 0.4 Ma (MSWD=0.23). Two younger and less concordant fractions likely underwent Pb loss.

4.2.5. Mesilinka equigranular granite: 04PSC-277

The sample is from the Mesilinka intrusive suite at the north end of the Hogem batholith, 21.8 km south-southeast of Johanson Lake and 21.2 km north-northwest of Horn Peak. It is a medium-grained equigranular biotite granite with a weak tectonic lineation and foliation.

Multi-grain fractions of zircon and titanite were analyzed. Two titanites yield a weighted mean $^{206}\text{Pb}/^{238}\text{U}$ date of 133.9 ± 0.3 Ma (MSWD =1.15), interpreted as a maximum crystallization age estimate. Three zircon fractions have results younger than titanites and are interpreted to have suffered from Pb loss. One zircon fraction is older than the titanites and discordant. This fraction is interpreted as inherited.

4.2.6. Mesilinka porphyritic granite: 04PSC-278

The sample is from the Mesilinka intrusive suite at the north end of the Hogem batholith, 21.3 km south-southeast of Johanson Lake, and 1 km west of sample 04PSC-277. It is a coarse-grained biotite granite, with scattered K-feldspar and plagioclase phenocrysts 1 to 2 cm long. The sample has a strong north-plunging lineation defined by elongate biotite clots and stretched feldspar and quartz grains, and a less-pronounced northeast-dipping tectonic foliation.

Multi-grain fractions of zircon and titanite were analyzed. Two zircon fractions yield a weighted mean $^{206}\text{Pb}/^{238}\text{U}$ date of 135.0 ± 0.3 Ma (MSWD =0.18). Two zircon fractions are slightly younger and likely have had Pb-loss. One zircon fraction is older and is interpreted as inherited or antecrystic. Two titanite fractions yield a weighted mean $^{206}\text{Pb}/^{238}\text{U}$ date of 134.5 ± 0.3 Ma (MSWD =0.89). This overlaps the two zircon fractions and is considered the time of crystallization.

4.2.7. Johanson Creek pluton: 04PSC-327

The Johanson Creek pluton, of mainly tonalite and quartz diorite, crops out west and northwest of Johanson Lake. It intrudes the Nicola Group and allied Triassic intrusions and is truncated to the west by the Ingenika fault. The sample, collected 6 km west of Johanson Lake and 600 m north of the Omineca Resource Access Road, is a medium-grained, equigranular biotite-hornblende tonalite with a weak tectonic foliation defined by mafic grains and tabular plagioclase grains.

Three multi-grain zircon fractions yield overlapping concordia ages with a weighted mean $^{206}\text{Pb}/^{238}\text{U}$ date of 130.8 ± 0.2 (MSWD=0.65). One older discordant fraction may have minor inheritance and one younger fraction may record Pb-loss. Two titanite fractions yield a similar, albeit slightly older weighted mean $^{206}\text{Pb}/^{238}\text{U}$ date of 131.0 ± 0.2 Ma (MSWD=0.89) and one other titanite is slightly younger.

4.2.8. Johanson Lake stock: 04PSC-329

The Johanson Lake stock, comprising monzonite, monzodiorite, and quartz monzonite, intrudes the Nicola Group northeast of Johanson Lake. The sample, collected 1 km north of the south end of Johanson Lake, is a medium-grained hornblende monzonite with 5% pink K-feldspar phenocrysts up to 1 cm long.

Two single zircon analyses from this sample yield a weighted mean $^{206}\text{Pb}/^{238}\text{U}$ date of 173.9 ± 0.3 Ma (MSWD=0.44) with two other younger results interpreted as the result of Pb-loss.

4.3.9. Unnamed diorite stock: 04PSC-330

The sample is from a small diorite stock that intrudes the Nicola Group southeast of Johanson Lake and is in turn cut by the Darb Creek pluton to the southwest. The sample is a medium-grained, equigranular hornblende diorite, strongly altered to chlorite and epidote, which was collected 2.5 km southeast of Johanson Lake and 1.4 km southwest of the Omineca Resource Access Road.

Three multi-grain zircon fractions yield overlapping concordia ages and the two more precise results yield a weighted mean $^{206}\text{Pb}/^{238}\text{U}$ date of 211.5 ± 0.3 Ma (MSWD=1.97). One fraction is older and interpreted as inherited.

4.4. LA-ICP-MS

Samples were collected by L. Ootes and G. Jones. Mineral separates were produced at the University of British Columbia and the University of Alberta. Zircons were picked by L. Ootes at the British Columbia Geological Survey and G. Jones at the University of Alberta. Zircon grain mounts were made at CCIM by G. Jones, R. Stern, and R. Dokken. The LA-ICP-MS work was conducted by G. Jones, A. Vezinet, and Y. Luo. Analysis of zircons in the samples with a 2018 prefix (e.g., 18lo12-7) were completed by split stream LA-ICP-MS, which included the concomitant acquisition of U-Pb and Lu-Hf isotopes (Table 3; Lu-Hf not reported in this study). Analysis of zircons in the samples with a 2019 prefix (e.g., 19GJ12-1), were completed by single stream LA-ICP-MS, which only included acquisition of U-Pb isotopes (Table 4). Zircons in sample 18lo22-1a were analyzed by single stream method. Data, graphical interpretations, data filtering processes, and supporting zircon images and descriptions are in Appendix 3, LA-ICP-MS.

4.4.1. U-Pb Filtering Methods for LA-ICP-MS

After LA-ICP-MS analysis and data reduction, U-Pb zircon data were filtered (Appendix 3) to remove zircons with $>1\%$ $f^{206}\text{Pb}_c$, indicating significant common lead (^{206}Pbc), from sample age calculations (Eqn. 1; e.g., Vezinet et al., 2018).

$$f^{206}\text{Pb}_c \% = [(^{206}\text{Pb}/^{204}\text{Pb})_{\text{Stacey \& Kramers, 1975}} / (^{206}\text{Pb}/^{204}\text{Pb})_{\text{measured}}] * 100 \quad (\text{Eqn. 1})$$

where ^{204}Pb measured is corrected for ^{204}Hg interference by subtracting the concentration of ^{202}Hg multiplied by the natural ratio of ^{204}Hg to ^{202}Hg from the concentration of ^{204}Pb . Zircons with $>10\%$ discordance were also filtered (Eqn. 2; Appendix 3).

$$\text{Discordance} (\%) = (1 - ^{206}\text{Pb}/^{238}\text{U} \text{ date} / ^{207}\text{Pb}/^{235}\text{U} \text{ date}) * 100 \quad (\text{Eqn. 2})$$

For zircons with supplementary trace element data, grains with concentrations of Ca >300 ppm, Fe >300 ppm, Ti >20 ppm, and La >1 ppm were filtered from sample age calculations (Appendix 3).

After filtering the zircon data using geochemistry and cathodoluminescent images, if the spread of the $^{206}\text{Pb}/^{238}\text{U}$ date of a sample yielded a mean squared weighted deviation (MSWD) of the weighted mean higher than statistically reasonable, the excessive scatter method (over-dispersion) was applied to the remaining data (Vermeesch, 2018). To reduce the spread in the data, an excess scatter constant was determined for each sample and added to the standard error of the individual analyses (Vermeesch, 2018), and new weighted mean $^{206}\text{Pb}/^{238}\text{U}$ dates were calculated using these greater uncertainties (Appendix 3). Standard error refers to the uncertainty of a sample, rather than standard deviation for uncertainty of a population. For samples that required excessive scatter, the robustness of the weighted mean $^{206}\text{Pb}/^{238}\text{U}$ date was shown by arbitrarily rejecting the youngest and oldest zircon dates in the sample to lower the MSWD, which yields a weighted mean $^{206}\text{Pb}/^{238}\text{U}$ age that overlaps with the excessive scatter weighted mean $^{206}\text{Pb}/^{238}\text{U}$ age (Appendix 3). A summary of the filtering applications and results for each sample are also in Appendix 3. An example of the filtering results and LA-ICP-MS U-Pb concordia plots are presented for Duckling Creek suite syenite sample 18lo25-2a in Appendix 3 and in Jones et al. (2021).

4.4.2. Results

4.4.2.1. Mesilinka tonalite: 19GJ12-1

The sample, from the Mesilinka suite 2.45 km northwest of Horn Peak, is of a grey, medium-grained, equigranular biotite-rich tonalite with a foliation defined by biotite. Equigranular granite dikes cut the tonalite in outcrop ~ 50 m away. The sample is mainly slightly altered plagioclase ($\sim 50\%$), with lesser strained quartz ($\sim 30\%$) and brown and green biotite ($\sim 15\%$). Subhedral amphibole and magnetite and anhedral epidote, apatite, and titanite are accessory and associated with patches of biotite.

The sample was analyzed by single stream LA-ICP-MS. After data filtering, the resulting weighted mean $^{206}\text{Pb}/^{238}\text{U}$ date is 134.1 ± 0.5 Ma ($n=18/23$; MSWD=1.49; probability of fit (pof)=0.09).

4.4.2.2. Thane Creek diorite: 19GJ12-4

The sample, collected 17.9 km east-northeast of Notch Peak, is a white and black, medium-grained, equigranular quartz diorite. It is mostly plagioclase ($\sim 62\%$), with about 25% equal parts green amphiboles with corroded clinopyroxene cores, and brown (metamorphic?) and green biotite. The sample contains minor quartz ($\sim 6\%$) and alkali feldspar ($\sim 7\%$), with accessory magnetite, apatite, titanite, and epidote. Titanite forms rims on magnetite grains. Trace fine-grained chalcopyrite is disseminated and forms inclusions in magnetite.

The sample was analyzed by single stream LA-ICP-MS. The weighted mean $^{206}\text{Pb}/^{238}\text{U}$ date is 206.6 ± 0.9 Ma ($n=10/13$; MSWD =1.77; pof=0.07).

4.4.2.3. Thane Creek suite: 18lo22-1a

The sample, collected 18.6 km south-southeast of Mount Ferris, is a coarse-grained to pegmatitic plagioclase-bearing

Table 3. 2018 Sample analysis, split stream LA-ICP-MS, U-Pb, and Lu-Hf (not reported in this study)

Laboratory & Sample Preparation	
Laboratory name	Arctic Resource Lab, University of Alberta (Canada)
Sample type/mineral	Zircon grains (magmatic)
Sample preparation	Conventional mineral separation, polished 1inch resin mount
Imaging	CL & BSE (Zeiss EVO MA15) 15kv, 3-5 nA
Laser ablation system	
Make, Model & type	RESolution ArF excimer
Ablation cell	Laurin Technic S-155
Laser wavelength	193 nm
Pulse width	4-20 ns
Fluence	ca. 6 J.cm ⁻² (120 mJ, 44% transmission)
Repetition rate	8 Hz
Ablation/Washout duration	45 secs / 45 secs
Ablation rate	0.125 μm.pulse ⁻¹ with the ca. 6.5 J.cm ⁻² setting
Spot diameter	44 μm
Sampling mode / pattern	Static spot ablation
Carrier gas	100% He in the cell, Ar and N ₂ make-up gas combined using a Y-piece 50% along the sample transport line to the torch.
Cell carrier gas flow	A mixture of 1.6-1.8 L/min Ar and 12-14ml/min N ₂ , which entered tangentially from the top of the S-155 ablation cell funnel and ~800 ml/min He entering from the side of the cell
ICP-MS Instruments	
U–Th–Pb measurements	
Make, Model & type	Thermo Fisher Scientific, Element XR, SC-SF-ICP-MS
Sample introduction	Ablation aerosol introduced through Tygon tubing
RF power	1360W
Detection system	202, 208, 232 in triple mode. 206 and 238 in analogue mode. 204 and 207 in counting mode 235 is calculated using canonical value. No Faraday cup used.
Masses measured	202, 204, 206, 207, 208, 232, 238
Integration time per peak/ dwell times	30 ms on 202, 204, 208 and 232; 60 ms on 206, 207 and 238
Total integration time	300 ms for each output datapoint
IC Dead time	20 ns
Data Processing	
Gas blank	30 second on-peak zero subtracted both for U-Pb and Lu-Hf measurements
Calibration strategy	91500 used as primary reference material (U-Pb), Plešovice, GJ-1, MUN1 & MUN-3 used as secondaries/validation materials.
Reference Material info	GJ-1 (Jackson et al., 2004; Morel et al., 2008) Plešovice (Sláma et al., 2008) MUN-1 and MUN-3 (Fisher et al., 2011) 91500 (Wiedenbeck et al., 1995; Wiedenbeck et al., 2004; Blichert-Toft, 2008)
Data processing package used / Correction for LIEF	Iolite software package (Paton et al., 2010; Paton et al., 2011; Fisher et al., 2017) using the following DRS: “U_Pb Geochron 4” for U–Th–Pb isotope analyses. LIEF correction assumes matrix match between reference material and samples.
Mass discrimination	Standard-sample bracketing with ²⁰⁷ Pb/ ²⁰⁶ Pb and ²⁰⁶ Pb/ ²³⁸ U normalized to primary reference material.
Common-Pb correction, composition and uncertainty	No common-Pb correction applied to the data
Uncertainty level & propagation	Ages are quoted at a coverage factor of 2, absolute. Propagation is by quadratic addition. Reproducibility and age uncertainty of reference material and common-Pb composition uncertainty are propagated where appropriate.

Table 4. 2019 Sample analysis, single stream LA-ICP-MS U-Pb zircon U-Pb, ThermoELEMENT II.

Laboratory and Sample Preparation	
Laboratory name	Arctic Resource Lab, University of Alberta (Canada)
Sample type/mineral	Zircon grains (magmatic)
Sample preparation	Conventional mineral separation, polished 1 inch resin mount
Imaging	CL & BSE (Zeiss EVO MA15) 15kv, 3-5 nA
Laser ablation system	
Make, Model & type	RESOLUTION ArF excimer
Ablation cell	Laurin Technic S-155
Laser wavelength	193 nm
Pulse width	4-20 ns
Fluence	~2 J.cm ⁻² (120 mJ, 11% transmission)
Repetition rate	6 Hz
Ablation/Washout duration	35 secs / 50-60 secs
Ablation rate	0.15 μm.pulse ⁻¹ with the <i>ca.</i> 1.3 J.cm ⁻² setting
Spot diameter	33 μm
Sampling mode / pattern	Static spot ablation
Carrier gas	A mixture of ~0.85 L/min Ar and 1ml/min N ₂ , which entered tangentially from the top of the S-155 ablation cell funnel and ~350 ml/min He entering from the side of the cell.
ICP-MS Instruments	
U–Th–Pb measurements	
Make, Model & type	Thermo Fisher Scientific, Element XR, SC-SF-ICP-MS
Sample introduction	Ablation aerosol introduced through Tygon tubing
RF power	1360W
Make-up gas flow (l/min)	Total gas is made of ~1.6 l.min ⁻¹ of Ar, 0.8-0.9 l.min ⁻¹ of He and 12-14 ml.min ⁻¹ of N ₂ . This total gas is divided between both ICP-MS at a ~ 50-50 rate.
Detection system	202, 208, 232 in triple mode. 206 and 238 in analogue mode. 204 and 207 in counting mode 235 is calculated using canonical value.
Masses measured	202, 204, 206, 207, 208, 232, 238
Integration time per peak/dwell times	30 ms on 202, 204, 208 and 232; 60 ms on 206, 207 and 238
Total integration time	300 ms for each output datapoint
IC Dead time	20 ns
Calibration strategy	91500 used as primary reference material (U-Pb), Plešovice and 94-35 used as secondaries/validation materials.
Reference Material info	Plešovice (Sláma et al., 2008) 91500 (Wiedenbeck et al., 1995; Wiedenbeck et al., 2004; Blichert-Toft, 2008) 94-35
Data processing package used / Correction for LIEF	Iolite software package (Paton et al., 2010; Paton et al., 2011; Fisher et al., 2017) using the following DRS: “ <i>U_Pb Geochron 4</i> ” for U–Th–Pb isotope analyses. LIEF correction assumes matrix match between reference material and samples.
Mass discrimination	Standard-sample bracketing with ²⁰⁷ Pb/ ²⁰⁶ Pb and ²⁰⁶ Pb/ ²³⁸ U normalized to primary reference material.
Common-Pb correction, composition and uncertainty	No common-Pb correction applied to the data
Uncertainty level & propagation	Ages are quoted at a coverage factor of 2, absolute. Propagation is by quadratic addition. Reproducibility and age uncertainty of reference material and common-Pb composition uncertainty are propagated where appropriate.

hornblende. Pegmatitic white hornblende-plagioclase segregations are interstitial to predominantly green hornblende. Hornblende is commonly overgrown by brown or green biotite, with biotite making up ~10% of the sample. The sample contains ~5% magnetite that is interstitial to amphibole and is abundant accessory titanite and apatite. Coarse, subhedral accessory epidote occurs in pegmatitic plagioclase segregations. Trace fine-grained chalcopyrite is disseminated through the sample.

The sample was analyzed by single stream LA-ICP-MS. The weighted mean $^{206}\text{Pb}/^{238}\text{U}$ date is 191.4 ± 0.7 Ma ($n=33/42$; MSWD=0.87; pof=0.68).

4.4.2.4. Thane Creek monzodiorite: 19GJ13-3

The sample, collected 25.9 km southeast of Notch Peak, is a 'salt and pepper', fine- to medium-grained, equigranular quartz monzodiorite. The sample contains ~40% euhedral plagioclase, ~30% poikilitic alkali feldspar, and ~15% anhedral, strained quartz. Mafic minerals make up ~10% of the sample, mainly subhedral amphibole (8%) with lesser biotite (2%). Magnetite, titanite, and apatite are accessory. Titanite occurs as ~1 mm anhedral grains and as fine rims on magnetite.

The sample was analyzed by single stream LA-ICP-MS. After data filtering, an excessive scatter constant of 3.99 was applied to the standard error of single data points to lower the MSWD of the weighted mean $^{206}\text{Pb}/^{238}\text{U}$ date. The resulting weighted mean $^{206}\text{Pb}/^{238}\text{U}$ age is 194.0 ± 1.1 Ma ($n=40/50$; MSWD=1.23; pof=0.16).

4.4.2.5. 18lo25-2a: Duckling Creek syenite

The sample, collected 22.7 km southeast of Notch Peak, is a pink-white, medium-grained, equigranular syenite consisting of ~90% two feldspars (K- and Na-bearing), with lesser clinopyroxene (~5%). Magnetite, titanite, and chlorite are the main accessory minerals. Titanite forms ~1 mm wide euhedral, wedge-shaped grains intergrown with clinopyroxene.

Two types of zircon were identified during mineral picking. 'Type one' zircons (Appendix 3; zircon images labelled 18lo25-2a z1) are clear-pink coloured fragments between 100 and 200 μm long. 'Type two' zircons (Appendix 3; zircon images labelled 18lo25-2a z2) are larger grains (300 to 400 μm) that are brown with good crystal habit. The cores of these zircons are commonly metamict or highly fractured. The results of U-Pb for both zircon types are included together.

The sample was analyzed by split stream LA-ICP-MS. After data filtering, an excessive scatter constant of 3.11 was applied to the standard error of single data points to lower the MSWD of the weighted mean $^{206}\text{Pb}/^{238}\text{U}$ date. The resulting weighted mean $^{206}\text{Pb}/^{238}\text{U}$ age is 178.9 ± 1.3 Ma ($n=22/44$; MSWD=1.33; pof=0.15).

4.4.2.6. 19GJ13-5a: Duckling Creek syenite

The sample was collected 31.1 km southwest of Notch Peak next to the Slide Cu-Au porphyry prospect, and 7 m south of a grab sample with chalcopyrite that yielded 0.07 wt.% Cu (19GJ13-5b; Ootes et al., 2020b). The sample is a pink-white and greenish-black, medium-grained, equigranular syenite. It contains alkali feldspar (~70%), with lesser amphibole (9%), plagioclase (8%), and clinopyroxene (5%). Biotite, chlorite, and magnetite combine to make up ~5% of the sample; fine-

grained apatite, titanite, and epidote are accessory minerals. Chalcopyrite occurs as rare fine, disseminated grains, and may be rimmed by titanite. The sample was analyzed by single stream LA-ICP-MS. The weighted mean $^{206}\text{Pb}/^{238}\text{U}$ date is 174.7 ± 0.7 Ma ($n=24/26$; MSWD=1.36; pof=0.12).

4.4.2.7. Osilinka granite: 18lo17-1

The sample, collected 11.89 km southeast of Notch Peak, is of a white (leucocratic), medium-grained, equigranular granite. Strained quartz (~37%), subhedral alkali feldspar (32%), and subhedral plagioclase (26%) comprise most of the sample. Accessory biotite, muscovite, and magnetite constitute less than 5% of the rock. Fine-grained biotite and magnetite occur interstitial to feldspar grains; muscovite is present within feldspar grain cores and between grain boundaries.

The sample was analyzed by split stream LA-ICP-MS. The thirteen remaining zircon grains after filtering are interpreted as inherited, and the youngest zircon has a $^{206}\text{Pb}/^{238}\text{U}$ date of 159.2 ± 4 Ma, interpreted as the maximum age for crystallization.

4.4.2.8. Sheet cutting Osilinka granite: 18lo20-4

The sample is from a flat-lying sheet, at least 4 m thick, that cuts the Osilinka suite, 14.01 km southeast of Notch Peak. Fine-grained plagioclase and quartz make up most of the groundmass, with plagioclase phenocrysts up to 0.5 cm. Magnetite, chlorite, epidote, and calcite are accessory in the groundmass. A ~0.5 mm wide calcite-filled vein cuts the sample. Rare, ~2.5 mm wide euhedral chalcopyrite grains occur in the groundmass.

The sample was analyzed by split stream LA-ICP-MS. After filtering, nine remaining analyses are interpreted as xenocrysts, and the youngest zircon has a $^{206}\text{Pb}/^{238}\text{U}$ date of 162.2 ± 2.6 Ma, interpreted as the maximum age for crystallization.

4.4.2.9. Mesilinka K-feldspar porphyritic granite: 18lo12-7

The sample, collected 2.06 km northeast of Horn Peak, is of a medium-grained K-feldspar porphyritic granite with a foliation defined by biotite. Clay-altered alkali feldspar (38%), strained anhedral quartz (28%), and myrmekitic plagioclase (22%) comprise most of the sample. Biotite (10%) is 1-2 mm wide and interstitial to feldspar and quartz. Accessory minerals include magnetite, apatite, epidote, and allanite with epidote rims.

The sample was analyzed by split stream LA-ICP-MS. After data filtering, an excessive scatter constant of 2.68 was applied to the standard error of single data points to lower the MSWD of the weighted mean $^{206}\text{Pb}/^{238}\text{U}$ date. The resulting weighted mean $^{206}\text{Pb}/^{238}\text{U}$ age is 134.8 ± 1.2 Ma ($n=14/33$; MSWD=1.64; pof=0.07).

4.4.2.10. Mesilinka equigranular granite: 18lo11-1

The sample, collected 1.48 km northeast of Horn Peak, is of equigranular, fine to medium-grained granite with a foliation defined by biotite. The sample is mostly strained fine-grained quartz (40%), anhedral medium-grained alkali feldspar (30%), and clay-altered plagioclase (25%). Accessory minerals include fine-grained muscovite, biotite, and magnetite. Magnetite is locally rimmed by titanite.

The sample was analyzed by split stream LA-ICP-MS. After data filtering, an excessive scatter constant of 2.34 was applied to the standard error of single data points to lower the MSWD

of the weighted mean $^{206}\text{Pb}/^{238}\text{U}$ date. The resulting weighted mean $^{206}\text{Pb}/^{238}\text{U}$ age is 127.9 ± 0.8 Ma ($n=23/48$; $\text{MSWD}=1.53$; $\text{pof}=0.05$).

5. $^{40}\text{Ar}/^{39}\text{Ar}$ Laser Step-Heating

Minerals for $^{40}\text{Ar}/^{39}\text{Ar}$ geochronology were separated at the British Columbia Geological Survey and a selection of hand-picked minerals sent to the University of Manitoba. Standards and unknowns were placed in 2 mm deep wells in 18 mm diameter aluminium disks, with standards placed strategically so that the lateral neutron flux gradients across the disk could be evaluated. Planar regressions were fit to the standard data, and the $^{40}\text{Ar}/^{39}\text{Ar}$ neutron fluence parameter, J , interpolated for the unknowns. All specimens were irradiated in the Cadmium-lined, in-core CLICIT facility of the Oregon State University TRIGA reactor. The duration of irradiation was 70 hours and used the Fish Canyon sanidine (28.201 Ma; Kuiper et al., 2008).

Irradiated samples were placed in a Cu sample tray, with a KBr cover slip, in a stainless-steel high vacuum extraction line and baked with an infrared lamp for 24 hours. All $^{40}\text{Ar}/^{39}\text{Ar}$ analytical work was performed using a multi-collector Thermo Fisher Scientific ARGUSVI mass spectrometer linked to a stainless steel Thermo Fisher Scientific extraction/purification line and Photon Machines (55 W) Fusions 10.6 CO₂ laser. Single crystals were either fused or step-heated using the laser, and reactive gases were removed, after ~ 3 minutes, by a JANIS cryocooler and three NP-10 SAES getters (two at room temperature and one at 450°C) before being admitted to an ARGUSVI mass spectrometer by expansion. Five argon isotopes were measured simultaneously over a period of 6 minutes. Measured isotope abundances were corrected for extraction-line blanks, which were determined before every sample analysis. Argon isotopes were measured using the following configuration: ^{40}Ar (H1; 1 x 1012 Ω resistor), ^{39}Ar (AX; 1 x 1013 Ω resistor), ^{38}Ar (L1; 1 x 1013 Ω resistor), ^{37}Ar (L2; 1 x 1013 Ω resistor) and ^{36}Ar (compact discrete dynode [CDD]). The sensitivity for argon measurements is $\sim 6.3 \times 10^{17}$ moles/fA as determined from measured aliquots of Fish Canyon Sanidine (Dazé et al., 2003; Kuiper et al., 2008).

Detector intercalibration (IC) between the different Faraday cups was monitored (in Qtegra) every two days by peak hopping ^{40}Ar . The intercalibration factor between H1 and the CDD was measured with the unknowns by online analysis of air pipettes (IC values can be found in Appendix 4). A value of 295.5 was used for the atmospheric $^{40}\text{Ar}/^{36}\text{Ar}$ ratio (Steiger and Jäger, 1977) for the purposes of routine measurement of mass spectrometer discrimination using air aliquots, and correction for atmospheric argon in the $^{40}\text{Ar}/^{39}\text{Ar}$ age calculation. Corrections are made for neutron-induced ^{40}Ar from potassium, ^{39}Ar and ^{36}Ar from calcium, and ^{36}Ar from chlorine (Roddick, 1983; Renne et al., 1998; Renne and Norman, 2001). Data collection and reduction were performed using Pylon (Ross, 2019). The decay constants used were those recommended by Min et al. (2000).

Samples were collected by L. Ootes. Mineral separation was at the British Columbia Geological Survey by L. Ootes and a selection of hand-picked minerals sent to the University of Manitoba. Further mineral preparation and Ar-Ar laser step-heating analyses was conducted by A. Camacho. Results are in Appendix 4 (Table “Ar-Ar data table” and “Ar-Ar figures”).

5.1. Results

The sample numbers in the headers in the data table and plots (Appendix 4) correspond to the rock sample number (e.g., 18lo22-1d), followed by lab number (e.g., 1889) and the Lab ID# corresponds to the individual laser step heating on the figures. The individual errors for each step are low. To calculate the age, a mean was calculated on the best analyses and the reported error is the 2 standard deviation of the mean. The steps used to calculate the age are shown in the plots and the amount of ^{39}Ar released during those steps is indicated (Appendix 4; Jones et al., 2021).

5.1.1. Thane Creek diorite: 18lo22-1d

The sample, also dated by U-Pb zircon by CA-TIMS (196.6 \pm 0.9 Ma, maximum crystallization age; section 4.1.3) was collected 18.6 km south-southeast of Mount Ferris. It is a medium-grained equigranular diorite with a moderate foliation defined by plagioclase and biotite and amphibole. The sample is mostly clay-altered plagioclase (65%), biotite (12%), and amphibole (6%). Minor altered alkali feldspar (7%) and quartz (1-2%) are present, interstitial to plagioclase. Accessory anhedral to subhedral, fine-grained epidote, apatite, and magnetite occur with biotite. Trace fine-grained chalcocopyrite is disseminated through the sample.

The sample yielded amphibole and biotite and two aliquots of each were tested by laser step heating. For hornblende, one aliquot yielded an age of 124 ± 2 Ma, the other an age of 124 ± 1 Ma. The two biotite aliquots gave ages of 126 ± 2 Ma, and 124 ± 1 Ma. The $^{40}\text{Ar}/^{39}\text{Ar}$ cooling age through the hornblende and biotite closure temperatures is estimated at 124 ± 1 Ma, which is interpreted to represent post-deformation cooling.

5.1.2. Thane Creek monzodiorite: 18lo26-1

The sample was collected from a site 3.69 km north of sample 19GJ13-3, which was dated by U-Pb zircon by LA-ICP-MS (194.0 \pm 1.1 Ma, section 4.4.2.4.). It consists of relatively pristine monzodiorite. One aliquot of hornblende yielded an age of 202 ± 5 Ma; a second failed to yield a result. We interpret 202 ± 5 Ma as a magmatic cooling age, recording when hornblende passed through its closure temperature.

5.1.3. Duckling Creek syenite: 18lo24-1

This sample is of coarse-grained equigranular monzonite (syenite) from the core of the Duckling Creek suite, 23.9 km south of Mount Ferris. The sample consists of coarse K-Feldspar (80%) with 15% mafic minerals, mainly medium-grained green clinopyroxene with lesser dark-green amphibole. Medium-grained titanite is intergrown with clinopyroxene, and accessory magnetite is disseminated throughout. The sample was collected 1.33 km northeast of sample 18lo25-2a, which gave a U-Pb zircon age by LA-ICP-MS (section 4.4.2.5.) Because 18lo25-2a did not yield hornblende, we collected sample 18lo24-1, from which hornblende was recovered. One aliquot yielded an age of 177 ± 5 Ma, a second failed to yield a result. The $^{40}\text{Ar}/^{39}\text{Ar}$ cooling age through the hornblende closure temperatures is estimated at 177 ± 5 Ma, which we interpret as a magmatic cooling age.

5.1.4. Osilinka granite: 18lo17-1

Also dated by U-Pb zircon by LA-ICP-MS (159.2 ± 4 Ma, section 4.4.2.7.), this sample of white (leucocratic), medium-grained, equigranular granite is from 12 km southeast of Notch Peak, in the core of the Osilinka granite. Strained quartz (~37%), subhedral alkali feldspar (32%), and subhedral plagioclase (26%) comprise most of the sample. Rare accessory biotite, muscovite, and magnetite constitute less than 5% of the rock. Fine-grained biotite and magnetite occur interstitial to feldspar grains, while muscovite is present within feldspar grain cores and boundaries.

Both muscovite and biotite were separated; one aliquot of muscovite yielded an age 122 ± 5 Ma, another failed to yield a result, one aliquot of biotite yielded an age of 116 ± 1 Ma. We interpret that these ages record post-ductile deformation cooling through closure temperatures.

5.1.5. Osilinka granite: 19ab5-6

This sample, from 7 km east of Notch Peak, is a leucocratic granite containing only rare biotite and muscovite. Both muscovite and biotite were separated from the sample; one aliquot of each failed to yield results that can be interpreted.

5.1.6. Mesilinka granodiorite: 18lo19-2

This sample, from 8.77 km south of Mount Ferris, is a medium-grained equigranular granodiorite with biotite and minor hornblende. One aliquot of biotite yielded an age 123 ± 2 Ma, one aliquot of hornblende failed to yield a result. This $^{40}\text{Ar}/^{39}\text{Ar}$ age is considered to record post-ductile deformation cooling through the biotite closure temperature.

5.1.7. Mesilinka tonalite: 18bg17-10

The sample was collected from 6.87 km south-southeast of Mount Ferris, within a body of medium-grained plagioclase-biotite tonalite that contains a foliation. The sample consists of 65% quartz and plagioclase with 30% mafic minerals. The mafic minerals are mostly green with lesser brown (metamorphic?) biotite and lesser euhedral hornblende. Titanite is an accessory mineral. One aliquot of biotite yielded a result of 108 ± 2 Ma, a second yielded an age of 111 ± 3 Ma. We consider that ca. 110 Ma provides an estimate for post-ductile deformation cooling through the biotite closure temperature.

5.1.8. Mesilinka K-feldspar porphyritic granite: 18lo12-7

The sample, collected 2.07 km northeast of Horn Peak, has a U-Pb zircon age of 134.8 ± 1.2 Ma (LA-ICP-MS; section 4.4.2.9.). The sample is of a porphyritic granite with K-feldspar phenocrysts (up to 5 cm) containing a biotite foliation that locally cuts the intrusive contact with Mesilinka equigranular granite. Clay-altered alkali feldspar phenocrysts up to 5 cm (38%), strained anhedral quartz (28%), and myrmekitic plagioclase (22%) comprise most of the sample. Biotite (10%) is 1-2 mm wide and interstitial to feldspar and quartz. Accessory minerals include magnetite, apatite, epidote, and allanite with epidote rims. One aliquot of biotite yielded an age of 112 ± 3 Ma, which we consider an estimate of post-ductile deformation cooling through the biotite closure temperature.

6. Detrital zircon U-Pb geochronology, trace elements, and Lu-Hf isotopes

6.1. Analytical techniques

6.1.1. U-Pb and trace elements

For detrital zircon U-Pb and trace element (TE) analysis, sample locations were carefully selected in the field and about two to 10 kg of rock were sampled from unaltered and lichen-free bedrock. Rock samples were sent to PCIGR at the University of British Columbia where they were crushed. Zircon separates were handpicked in alcohol and mounted in epoxy along with reference materials. Grain mounts were then wet-ground with carbide abrasive paper and polished with diamond paste. Cathodoluminescence (CL) imaging was carried out on a Philips XL-30 scanning electron microscope (SEM) equipped with a Bruker Quanta 200 energy-dispersion X-ray microanalysis system at the Electron Microbeam/X-Ray Diffraction Facility (EMXDF; Appendix 5). An operating voltage of 15 kV was used, with a spot diameter of 6 μm and peak count time of 17-27 seconds. After removal of the carbon coat, the grain mount surface was washed with mild soap and rinsed with high-purity water. Before analysis, the grain mount surface was cleaned with 3 N HNO_3 acid and again rinsed with high-purity water to remove any surface Pb contamination that could interfere with the early portions of the spot analyses.

Analyses were conducted using a Resonetics RESolution M-50-LR, which contains a Class I laser device equipped with a UV excimer laser source (Coherent COMPex Pro 110, 193 nm, pulse width of 4 ns) and a two-volume cell designed and developed by Laurin Technic Pty. Ltd. (Australia). This sample chamber allowed for the investigation of several grain mounts during one analytical session. The laser path was fluxed by N_2 to ensure better stability. Ablation was carried out in a cell with a volume of approximately 20 cm^3 and a He gas stream that ensured better signal stability and lower U-Pb fractionation (Eggins et al., 1998). The laser cell was connected via a Teflon squid to an Agilent 7700x quadrupole ICP-MS housed at PCIGR. A pre-ablation shot was used to ensure that the spot area on grain surface was contamination-free. Samples and reference materials were analyzed for 36 isotopes: ^7Li , ^{29}Si , ^{31}P , ^{43}Ca , ^{45}Sc , ^{49}Ti , Fe (^{56}Fe , ^{57}Fe), ^{89}Y , ^{91}Zr , ^{93}Nb , Mo (^{95}Mo , ^{98}Mo), ^{139}La , ^{140}Ce , ^{141}Pr , ^{146}Nd , ^{147}Sm , ^{153}Eu , ^{157}Gd , ^{159}Tb , ^{163}Dy , ^{165}Ho , ^{166}Er , ^{169}Tm , ^{172}Lu , ^{177}Hf , ^{181}Ta , ^{202}Hg , Pb (^{204}Pb , ^{206}Pb , ^{207}Pb , ^{208}Pb), ^{232}Th , and U (^{235}U , ^{238}U) with a dwell time of 0.02 seconds for each isotope. Pb/U and Pb/Pb ratios were determined on the same spots along with trace element concentration determinations. These isotopes were selected based on their relatively high natural abundances and absence of interferences. The settings for the laser were: spot size of 34 μm with a total ablation time of 30 seconds, frequency of 5 Hz, fluence of 5 J/cm^2 , power of 7.8 mJ after attenuation, pit depths of approximately 15 μm , He flow rate of 800 mL/min, N_2 flow rate of 2 mL/min., and a carrier gas (Ar) flow rate of 0.57 L/min.

Reference materials were analyzed throughout the sequence to allow for drift correction and to characterize downhole fractionation for Pb/U and Pb/Pb isotopic ratios. For trace elements, NIST 612 glass was used for both drift correction and trace element calibration, with sample spacing between every five to eight unknowns; ^{90}Zr was used as the internal

standard assuming stoichiometric values for zircon. NIST 610 glass was analyzed after each NIST 612 analysis and used as a monitor reference material for trace elements. For U-Pb analyses, natural zircon reference materials were used, including Plešovice (337.13 ± 0.33 Ma; Sláma et al., 2008) or 91500 (1065 Ma; Wiedenbeck et al., 1995, 2004) for internal reference, and both Temora2 (416.78 ± 0.33 Ma; Black et al., 2004) and Plešovice and/or 91500 for monitoring. The zircon reference materials were placed between the unknowns in a similar fashion as the NIST glasses. Raw data were reduced using the Iolite 3.4 extension (Paton et al., 2011) for Igor Pro™ yielding concentration values, Pb/U and Pb/Pb dates, and their respective propagated uncertainties. Final interpretation and plotting of the analytical results employed the ISOPLOT software of Ludwig (2003).

Sampling was conducted by L. Ootes, D. Milidragovic, and G. Jones. At PCIGR, R. Friedman oversaw zircon separation and analyses. Results are Appendix 5 (Table “LA-ICPMS_detrizircon_U_Pb_TE”).

6.1.2. Lu-Hf isotopes

After detrital zircon U-Pb and TE analyses, zircon grain mounts were sent to the Arctic Resources Laboratory at the University of Alberta. Laser ablation-MC-ICP-MS Lu-Hf isotopic analysis of zircon was conducted by L. Ootes and Y. Luo. Instrumentation and analytical details are given in Table 5. Plešovice zircon was used as a primary reference material (Sláma et al., 2008). In this study we monitored the Yb interference correction, and the measured ¹⁷⁶Yb/¹⁷³Yb was iteratively calibrated to optimize the Yb-interference correction, monitored by zircon reference materials with variable Yb contents (91500, MUN1 and MUN3). Multiple analyses (n = 23) of the 91500 zircon standard (Blichert-Toft, 2008) yielded a weighted mean ¹⁷⁶Hf/¹⁷⁷Hf of 0.282313 ± 52 (2 SD). The results agree with the ¹⁷⁶Hf/¹⁷⁷Hf value of 0.282308 ± 6 (2 SD; Blichert-Toft, 2008). The mean ¹⁷⁶Hf/¹⁷⁷Hf for MUN1 and MUN3 (0.282135 ± 33 [2 SD], n = 42; 0.282130 ± 47 [2 SD], n = 33) are in good agreement with the solution MC-ICP-MS values of 0.282135 ± 31 (2 SD) for MUNZirc 1

Table 5. Laser ablation system for Lu-Yb-Hf measurements.

Laser ablation system									
Make, Model & type	RESOLUTION ArF excimer								
Ablation cell	Laurin Technic S-155								
Laser wavelength	193 nm								
Pulse width	20 ns								
Fluence	ca. 6.5 J.cm ⁻² (120 mJ, 44% transmission)								
Repetition rate	8 Hz								
Ablation/Washout duration	60 secs / 60 secs								
Ablation rate	0.125 μm.pulse ⁻¹ with the ca. 6.5 J.cm ⁻² setting								
Spot diameter	33 μm								
Sampling mode / pattern	Static spot ablation								
Carrier gas and gas flow	A mixture of ~0.85 L/min Ar and 6- 7 ml/min N ₂ , which entered tangentially from the top of the S-155 ablation cell funnel and ~400 ml/min He entering from the side of the cell.								
Lu–Yb–Hf measurements									
Make, Model & type	Thermo Fisher Scientific, Neptune Plus, MC-SF-ICP-MS								
Sample introduction	Ablation aerosol introduced tygon tubing. Ni-Jet Sample cone and X-Skimmer cone.								
RF power	1250W								
Detection system	Static Faraday (attached to 10 ¹¹ Ω amplifier) measurement								
Masses measured	172, 173, 175, 176, 177, 178, 179, 180, 181								
Total integration time per output datapoint	1.049 secs								
Cup configuration	L4	L3	L2	L1	Axial	H1	H2	H3	H4
	172	173	175	176	177	178	179	180	181
Data Processing									
Gas blank	60 second on-peak zero subtracted for Lu-Hf measurements								
Reference Material info	Plešovice (Sláma et al., 2008) 91500 (Blichert-Toft, 2008) MUN-1 and MUN-3 (Fisher et al., 2011)								
Data processing package used	Iolite software package (Paton <i>et al.</i> , 2010; Paton <i>et al.</i> , 2011; Fisher <i>et al.</i> , 2017) using the following DRS: ““ <i>Hf Alberta</i> ”								
Yb mass bias coefficient (β^{Yb})	Calculated using ¹⁷³ Yb/ ¹⁷² Yb invariant ratio and the exponential law of Russell et al. (1978).								
Yb interference	Calculated with ¹⁷⁶ Yb/ ¹⁷³ Yb ratio, the Yb-mass bias coefficient (β^{Yb}) and the exponential law of Russell et al. (1978). Daily adjusted.								
Lu interference	Calculated with ¹⁷⁶ Lu/ ¹⁷⁵ Lu ratio, the Yb-mass bias coefficient (β^{Yb}) and the exponential law of Russell et al. (1978). Daily adjusted.								

and 3 (Fisher et al., 2011). The decay constant and parameters used for Hf model age calculations are $^{176}\text{Hf}/^{177}\text{Hf}$ (chondrite) = 0.0336, $^{176}\text{Hf}/^{177}\text{Hf}$ = 0.282785 (chondrite) after Bouvier et al. (2008) and $^{176}\text{Hf}/^{177}\text{Hf}$ (Depleted Mantle) = 0.038, $^{176}\text{Hf}/^{177}\text{Hf}$ = 0.283223 (Depleted Mantle) after Vervoort and Blichert-Toft (1999). Uncertainties on initial Hf ratios and epsilon Hf values were calculated using full error propagation, outlined by Ickert (2013). Results and zircon CL images are in Appendix 5.

6.2. Results

Detrital zircon U-Pb, Lu-Hf, and trace element results and CL images of each grain mount are in Appendix 5. The sample numbers in the data tables correspond to the rock sample number, followed by zircon grain identification code that is also labelled on the CL images. Maximum deposition ages are estimated using the TuffZirc application in Isoplot (Ludwig, 2003) and weighted averages of the youngest cluster of two or more grain ages overlapping in age at 1 sigma.

6.2.1. Asitka Group: 19lo14-5

The sample was collected ~ 2.2 km west-southwest of Mount Carruthers peak and approximately 280 m above the base and 280 m below the top of the Asitka Group exposure at this location. It is a quartzose sandstone with pebbles of quartz and other rocks. The sandstone is 4 m thick. The sandstone unit overlies and underlies black shale, and all rocks contain a strong foliation. The maximum deposition age from 57 zircons is estimated at ca. 323 Ma.

6.2.2. Sitlika assemblage: DMI19-9-12

The sample, collected 14km south-southeast of Axelgold Peak and 6.3 km east-northeast of Nankai Peak, is of a grey, fine-grained feldspathic sandstone that is biotite rich and strongly foliated. The sandstone is interbedded with fissile mudstone. The maximum deposition age from a subset of 34 zircons is estimated at ca. 218 Ma. This sample also contains older populations of ca. 245 and ca. 325 Ma zircons.

6.2.3. Telkwa Formation (Hazelton Group): 19GJ18-3

The sample, collected 6.3 km southeast of Mount Carruthers peak, is of a white to purple, fine-grained feldspathic sandstone that is strongly foliated. The sandstone is in a sedimentary unit that contains monomictic and polymictic pebble-cobble conglomerates and green and purple shales. The maximum deposition age from 62 zircons is estimated at ca. 196 Ma.

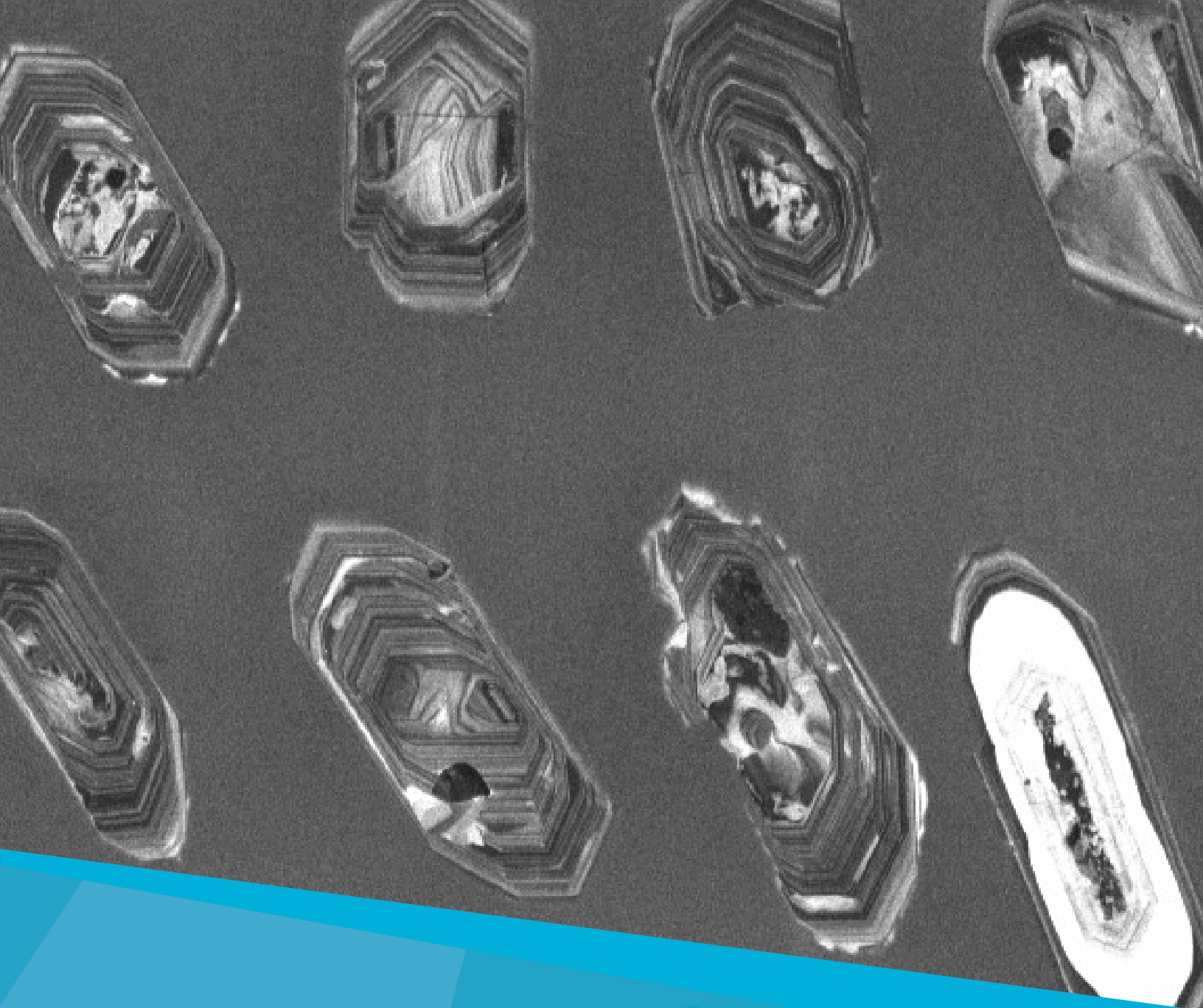
Acknowledgements

Sample preparation for whole-rock geochemistry benefited from the assistance of R. Simmonds. The zircon CA-TIMS analyses at PCIGR was assisted by H. Lin, who did the mineral separation and assisted with mass spectrometry, and T. Ockerman, who conducted activities in the clean lab. For detrital zircon LA-ICP-MS analyses at PCIGR, M. Amini was in charge of LA-ICP-MS analysis and assisted by H. Lin and T. Ockerman who conducted sample preparation and data reduction. We are grateful for field assistance from A. Bergen, B. Graham, R. Simmonds, D. Spence, S. Rauhala, K. Shortridge, M. Farhat, and J. Lockie.

References cited

- Black, L.P., Kamo, S.L., Allen, C.M., Davis, D.W., Aleinikoff, J.N., Mundil, R., Campbell, I.H., Korsch, R.J., Williams, I.S., and Foudoulis, C., 2004. Improved $^{206}\text{Pb}/^{238}\text{U}$ microprobe geochronology by the monitoring of a trace-element-related matrix effect; SHRIMP, ID-TIMS, ELA-ICP-MS and oxygen isotope documentation for a series of zircon standards. *Chemical Geology*, 205, 115-140.
- Blichert-Toft, J., 2008 The Hf isotopic composition of zircon reference material 91500. *Chemical Geology*, 253, 252-257.
- Bouvier, A., Vervoort, J.D. and Patchett, P J., 2008. The Lu-Hf and Sm-Nd isotopic composition of CHUR: Constraints from unequilibrated chondrites and implications for the bulk composition of terrestrial planets: *Earth and Planetary Science Letters*, 273, 48-57.
- CGG Canada Services Ltd., 2018. Geophysical survey report MIDAS high resolution magnetic and radiometric survey Search Project Phase III. *Geoscience BC Report 2018-2*.
- Cousens, B.L., 1996. Magmatic evolution of Quaternary mafic magmas at Long Valley Caldera and the Devils Postpile, California: Effects of crustal contamination on lithospheric mantle-derived magmas. *Journal of Geophysical Research: Solid Earth* 101 (B12), 27673-27689
- Crowley, J.L., Schoene, B., and Bowring, S.A., 2007. U-Pb dating of zircon in the Bishop Tuff at the millennial scale. *Geology*, 35, 1123-1126.
- Dazé, A., Lee, J.K.W., and Villeneuve, M., 2003. An intercalibration study of the Fish Canyon sanidine and biotite $^{40}\text{Ar}/^{39}\text{Ar}$ standards and some comments on the age of the Fish Canyon Tuff. *Chemical Geology*, 199, 111-127.
- Eggins, S.M., Kinsley, L., and Shelley, J., 1998. Deposition and element fractionation processes during atmospheric pressure laser sampling for analysis by ICP-MS. *Applied Surface Science*, 127-129, 278-286.
- Fisher, C.M., Hanchar, J.M., Samson, S.D., Dhuime, B., Blichert-Toft, J., Vervoort, J.D., and Lam, R., 2011. Synthetic zircon doped with hafnium and rare earth elements: A reference material for in situ hafnium isotope analysis. *Chemical Geology*, 286, 32-47.
- Fisher, C.M., Vervoort, J.D., and Hanchar, J. M., 2014. Guidelines for reporting zircon Hf isotopic data by LA-MC-ICPMS and potential pitfalls in the interpretation of these data. *Chemical Geology*, 363, 125-133.
- Fisher, C.M., Paton, C., Pearson, D.G., Sarkar, C., Luo, Y., Tersmette, D.B. and Chacko, T., 2017. Data reduction of Laser Ablation Split-Stream (LASS) analyses using newly developed features within Iolite: With applications to Lu-Hf+ U-Pb in detrital zircon and Sm-Nd+ U-Pb in igneous monazite. *Geochemistry, Geophysics, Geosystems*, 18, 4604-4622.
- Gerstenberger, H., and Haase, G., 1997. A highly effective emitter substance for mass spectrometric Pb isotopic ratio determinations. *Chemical Geology*, 136, 309-312.
- Ickert, R.B., 2013. Algorithms for estimating uncertainties in initial radiogenic isotope ratios and model ages. *Chemical Geology*, 340, 131-138.
- Jackson, S.E., Pearson, N.J., Griffin, W.L., and Belousova, E.A., 2004. The application of laser ablation-inductively coupled plasma-mass spectrometry to in-situ U-Pb zircon geochronology. *Chemical Geology*, 211, 47-69.
- Jaffey, A.H., Flynn, K.F., Glendenin, L.E., Bentley, W.C., and Essling, A.M., 1971. Precision measurement of half-lives and specific activities of ^{235}U and ^{238}U . *Physical Review C*, 4, 1889-1906.
- Jones, G., Ootes, L., Milidragovic, D., Friedman, R., Camacho, A., Luo, Y., Vezinet, A., Pearson, D.G., Schiarizza, P., 2021. Geochronology of northern Hogen batholith, Quesnel terrane, north-central British Columbia. In: *Geological Fieldwork 2020*, British Columbia Ministry of Energy, Mines and Low Carbon

- Innovation British Columbia Geological Survey Paper 2021-01, in press.
- Kuiper, K.F., Deino, A., Hilgen, F.J., Krijgsman, W., Renne, R., and Wijbrans, J.R., 2008. Synchronizing rock clocks of Earth history. *Science*, 320, 500-504.
- Krogh, T.E., 1982. Improved accuracy of U-Pb zircon ages by the creation of more concordant systems using an air abrasion technique. *Geochimica et Cosmochimica Acta*, 46, 637-649.
- Ludwig, K. R., 2003. Isoplot 3.00, A Geochronological Toolkit for Microsoft Excel. University of California at Berkeley.
- Mattinson, J.M., 2005. Zircon U-Pb chemical abrasion ("CA-TIMS") method: Combined annealing and multi-step partial dissolution analysis for improved precision and accuracy of zircon ages. *Chemical Geology*, 220, 47-66.
- Min, K., Mundil, R., Renne, P.R., and Ludwig, K.R., 2000. A test for systematic errors in $^{40}\text{Ar}/^{39}\text{Ar}$ geochronology through comparison with U/Pb analysis of a 1.1-Ga rhyolite. *Geochimica et Cosmochimica Acta*, 64, 73-98.
- Monger, J.W.H., 1977. The Triassic Takla Group in McConnell Creek map-area, north-central British Columbia. Geological Survey of Canada, Paper 76-29, 45 p.
- Morel, M. L. A., Nebel, O., Nebel-Jacobsen, Y. J., Miller J. S., and Vroon, P. Z., 2008. Hafnium isotope characterization of the GJ-1 zircon reference material by solution and laser-ablation MC-ICPMS. *Chemical Geology*, 255, 231-235.
- Mundil, R., Ludwig, K. R., Metcalfe, I., and Renne, P. R., 2004. Age and timing of the Permian mass extinctions: U/Pb dating of closed-system zircons. *Science*, 305, 1760-1763.
- Ootes, L., Bergen, A.L., Milidragovic, D., Graham, B., and Simmonds, R., 2019. Preliminary geology of northern Hogen batholith, Quesnel terrane, north-central British Columbia; In: Geological Fieldwork 2018, British Columbia Ministry of Energy, Mines and Petroleum Resources British Columbia Geological Survey Paper 2019-01, pp. 31-53.
- Ootes, L., Bergen, A.L., Milidragovic, D., and Jones, G.O., 2020a. Bedrock geology of the northern Hogen batholith and its surroundings, north-central British Columbia. British Columbia Ministry of Energy and Mines and Petroleum Resources, British Columbia Geological Survey Open File 2020-02, scale 1:50,000.
- Ootes, L., Bergen, A.L., Milidragovic, D., Jones, G.O., Camacho, A., and Friedman, R., 2020b. An update on the geology of northern Hogen batholith and its surroundings, north-central British Columbia. In: Geological Fieldwork 2019, British Columbia Ministry of Energy, Mines and Petroleum Resources, British Columbia Geological Survey Paper 2020-01, pp. 25-47.
- Parrish, R., Roddick, J.C., Loveridge, W.D., and Sullivan, R.W., 1987. Uranium-lead analytical techniques at the geochronology laboratory, Geological Survey of Canada. In: Radiogenic Age and Isotopic Studies, Report 1, Geological Survey of Canada, Paper 87-2, pp. 3-7.
- Paton, C., Woodhead, J. D., Hellstrom, J. C., Hergt, J. M., Greig, A. and Maas, R., 2010. Improved laser ablation U-Pb zircon geochronology through robust downhole fractionation correction. *Geochimica et Cosmochimica Acta*, 74, 303-313. doi: 10.1016/j.gca.2009.12.018.
- Paton, C., Hellstrom, J., Paul, B., Woodhead, J., and Hergt, J., 2011. Iolite: Freeware for the visualization and processing of mass spectrometric data. *Journal of Analytical Atomic Spectrometry*, 26, 2508-2518.
- Renne, P.R., and Norman, E.B., 2001. Determination of the half-life of ^{40}Ar by mass spectrometry. *Physical Review C*, 63, 047302, 3 p.
- Renne, P.R., Swisher, C.C., Deino, A.L., Karner, D.B., Owens, T.L. and DePaolo, D.J., 1998. Intercalibration of standards, absolute ages and uncertainties in $^{40}\text{Ar}/^{39}\text{Ar}$ dating. *Chemical Geology*, 145, 117-152.
- Richard, P., Shimizu, N., and Allègre, C.J., 1976. $^{143}\text{Nd}/^{146}\text{Nd}$, a natural tracer: An application to oceanic basalts. *Earth and Planetary Science Letters*, 31, 269-278.
- Roddick, J.C., 1983. High precision intercalibration of $^{40}\text{Ar}-^{39}\text{Ar}$ standards. *Geochimica Cosmochimica Acta*, 47, 887-898.
- Ross, J., 2019. NMGR/psychron v18.2: doi: 10.5281/zenodo.3237834.
- Schiarizza, P., and Tan, S.H., 2005. Geology of the Johanson Lake area, parts of NTS 94D/8 and 9. British Columbia Ministry of Energy, Mines and Petroleum Resources, British Columbia Geological Survey Open File 2005-4, scale 1:50,000.
- Schmitz, M.D., and Schoene, B., 2007. Derivation of isotope ratios, errors, and error correlations for U-Pb geochronology using $^{205}\text{Pb}-^{235}\text{U}$ (^{233}U)-spiked isotope dilution thermal ionization mass spectrometric data. *Geochemistry, Geophysics, Geosystems*, 8, https://doi.org/10.1029/2006GC001492.
- Scoates, J.S., and Friedman, R.M. 2008. Precise age of the platinumiferous Merensky Reef, Bushveld Complex, South Africa, by the U-Pb ID-TIMS chemical abrasion ID-TIMS technique. *Economic Geology*, 103, 465-471.
- Sláma, J., Košler, J., Condon, D. J., Crowley, J. L., Gerdes, A., Hanchar, J. M., Horstwood, M. S. A., Morris, G. A., Nasdala, L., Norberg, N., Schaltegger, U., Schoene, B., Tubrett, M. N. and Whitehouse, M. J., 2008. Plešovice zircon - A new natural reference material for U-Pb and Hf isotopic microanalysis. *Chemical Geology*, 249, 1-35.
- Stacey, J.S., and Kramers, J.D., 1975. Approximation of terrestrial lead isotopic evolution by a two-stage model. *Earth and Planetary Science Letters*, 26, 207-221.
- Steiger, R.H., and Jäger, E., 1977. Subcommittee on geochronology: Convention on the use of decay constants in geo- and cosmochronology. *Earth and Planetary Science Letters*, 36, 359-362.
- Tanaka, T., Togashi, S., Kamioka, H., Amakawa, H., Kagami, H., Hamamoto, T., Yuhara, M., Orihashi, Y., Yoneda, S., Shimizu, H., Kunimaru, T., Takahashi, K., Yanagi, T., Nakano, T., Fujimaki, H., Shinjo, R., Asahara, Y., Tanimizu, M., and Dragusanu, C., 2000. JNdi-1: A neodymium isotopic reference in consistency with LaJolla neodymium. *Chemical Geology*, 168, 279-281.
- Thirlwall, M.F., 2000. Inter-laboratory and other errors in Pb isotope analyses investigated using a $^{207}\text{Pb}-^{204}\text{Pb}$ double spike. *Chemical Geology*, 163, 299-322.
- Vermeesch, P., 2018. IsoplotR: A free and open toolbox for geochronology. *Geoscience Frontiers*, 9, 1479-1493.
- Vervoort, J.D., and Blichert-Toft, J., 1999. Evolution of the depleted mantle: Hf isotope evidence from juvenile rocks through time. *Geochimica et Cosmochimica Acta*, 63, 533-556.
- Vezinet, A., Pearson, D.G., Thomassot, E., Stern, R.A., Sarkar, C., Luo, Y., and Fisher, C.M., 2018. Electronic Supplementary Material: Hydrothermally-altered mafic crust as source for early Earth TTG: Pb/Hf/O isotope and trace element evidence from TTG of the Eoarchean Saglek Block, N. Labrador. *Earth and Planetary Science Letters*, 503, 95-107.
- Wiedenbeck, M., Alle, P., Corfu, F., Griffin, W.L., Meier, M., Oberli, F., Quadt, A.V., Roddick, J.C., and Spiegel, W., 1995. Three natural zircon standards for U-Th-Pb, Lu-Hf, trace element and REE analyses. *Geostandards Newsletter*, 19, 1-23.
- Wiedenbeck, M., Hanchar, J.M., Peck, W.H., Sylvester, P., Valley, J., Whitehouse, M., Kronz, A., Morishita, Y., Nasdala, L., Fiebig, F., Franchi, I., Girard, J.P., Greenwood, R.C., Hinton, R., Kita, N., Mason, P.R.D., Norman, M., Ogasawara, M., Piccoli, P.M., Rhede, D., Satoh, H., Schulz-Dobrick, B., Skår, Ø., Spicuzza, M.J., Terada, K., Tindle, K., Togashi, S., Vennemann, T., Xie, Q. and Zheng, Y.F., 2004. Further characterization of the 91500 zircon crystal. *Geostandards Geoanalytical Research*, 28, 9-39.



Ministry of
Energy, Mines and
Low Carbon Innovation

